AMERICAN JOURNAL OF PHYSIOLOGY
GASTROINTESTINAL AND LIVER PHYSIOLOGY

Am J Physiol Gastrointest Liver Physiol 323: G571–G585, 2022.
First published October 4, 2022; doi:10.1152/ajpgi.00121.2022

RESEARCH ARTICLE

Inter-Organ Communication in Homeostasis and Disease

IMP1/IGF2BP1 in human colorectal cancer extracellular vesicles

Madeline Kuhn,[1] Yang Zhang,[1] John Favate,[5] Mayu Morita,[2] Aurora Blucher,[3] Sukanya Das,[5] Shun Liang,[5] Ranjan Preet,[6] Louis R. Parham,[7] Kathy N. Williams,[8] Sudheer Molugu,[9] Randall J. Armstrong,[3,4] Wei Zhang,[10] Jiegang Yang,[10] Kathryn E. Hamilton,[7] Dan A. Dixon,[6] Gordon Mills,[3] Terry K. Morgan,[2,4] Premal Shah,[5] and Sarah F. Andres[1]

[1]*Pediatric Gastroenterology Division, Department of Pediatrics, School of Medicine, Oregon Health and Science University, Portland, Oregon;* [2]*Department of Pathology, Oregon Health and Science University, Portland, Oregon;* [3]*Division of Oncological Sciences, Knight Cancer Institute, Oregon Health and Science University, Portland, Oregon;* [4]*Cancer Early Detection Advanced Research, Oregon Health and Science University, Portland, Oregon;* [5]*Department of Genetics, Rutgers University, Piscataway, New Jersey;* [6]*Department of Molecular Biosciences, University of Kansas Cancer Center, University of Kansas, Lawrence, Kansas;* [7]*Division of Gastroenterology Hepatology and Nutrition, Children's Hospital of Philadelphia, University of Pennsylvania Perelman School of Medicine, Philadelphia, Pennsylvania;* [8]*Division of Gastroenterology, Department of Medicine, Abramson Cancer Center, University of Pennsylvania Perelman School of Medicine, Philadelphia, Pennsylvania;* [9]*Electron Microscopy Resource Lab, University of Pennsylvania Perelman School of Medicine, Philadelphia, Pennsylvania; and* [10]*Department of Biology, University of Pennsylvania, Philadelphia, Pennsylvania*

Abstract

Colorectal cancer (CRC) is a leading cause of cancer-related death. There is an urgent need for new methods of early CRC detection and monitoring to improve patient outcomes. Extracellular vesicles (EVs) are secreted, lipid-bilayer bound, nanoparticles that carry biological cargo throughout the body and in turn exhibit cancer-related biomarker potential. RNA binding proteins (RBPs) are posttranscriptional regulators of gene expression that may provide a link between host cell gene expression and EV phenotypes. Insulin-like growth factor 2 RNA binding protein 1 (IGF2BP1/IMP1) is an RBP that is highly expressed in CRC with higher levels of expression correlating with poor prognosis. IMP1 binds and potently regulates tumor-associated transcripts that may impact CRC EV phenotypes. Our objective was to test whether IMP1 expression levels impact EV secretion and/or cargo. We used RNA sequencing, in vitro CRC cell lines, ex vivo colonoid models, and xenograft mice to test the hypothesis that IMP1 influences EV secretion and/or cargo in human CRC. Our data demonstrate that IMP1 modulates the RNA expression of transcripts associated with extracellular vesicle pathway regulation, but it has no effect on EV secretion levels in vitro or in vivo. Rather, IMP1 appears to affect EV regulation by directly entering EVs in a transformation-dependent manner. These findings suggest that IMP1 has the ability to shape EV cargo in human CRC, which could serve as a diagnostic/prognostic circulating tumor biomarker.

NEW & NOTEWORTHY This work demonstrates that the RNA binding protein IGF2BP1/IMP1 alters the transcript profile of colorectal cancer cell (CRC) mRNAs from extracellular vesicle (EV) pathways. IMP1 does not alter EV production or secretion in vitro or in vivo, but rather enters CRC cells where it may further impact EV cargo. Our work shows that IMP1 has the ability to shape EV cargo in human CRC, which could serve as a diagnostic/prognostic circulating tumor biomarker.

colorectal adenocarcinoma; exosome; liquid biopsy; RNA binding protein

INTRODUCTION

Colorectal cancer (CRC) is the third most common cancer worldwide, accounting for 10% of all newly diagnosed cancer cases (1, 2). Despite decreases in CRC diagnoses in older adults (>50 yr), the incidence of CRC in younger patients (<50 yr) is rising (3), with reduced access to preventative care and screening predicted to elevate death rates from CRC over the next decade (4).

Early diagnosis is critical for proper treatment and long-term patient survival, which is >90%, if CRC is detected at an early stage (2). Colonoscopy and histopathological diagnoses of tissue biopsies are the current clinical gold standard (5). However, this approach is invasive, expensive, highly

Correspondence: S. F. Andres (andress@ohsu.edu).
Submitted 10 May 2022 / Revised 22 September 2022 / Accepted 27 September 2022

dependent on the skill of the endoscopist impacting sensitivity, and a tissue biopsy may not account for tumor heterogeneity that impacts treatment choices and prognosis (6, 7).

Tumor biomarker analyses of liquid biopsies (e.g., plasma) have promise for early cancer detection with broad molecular phenotyping of tumor heterogeneity (6, 8–10). Tumor biomarkers may include circulating tumor cells, cell-free DNA, RNA, or proteins. In addition, extracellular vesicles, (EVs) released by tumor cells and/or the patient's host response are another emerging source of sensitive and specific biomarkers, in part because they are present in relative high concentrations within plasma ($\sim 10^{10}$/mL) (11). In turn, regulation of EV synthesis, their cargo, secretion, and tumor-related phenotypes are the subject of intense interest (12–21). EVs are lipid bilayer-encased nanoparticles released from cells to carry biological cargo as intercellular signals (13). EVs carry lipids, proteins, and RNAs that can facilitate tumor progression and metastasis (14–16). EV phenotypes could therefore prove to be useful biomarkers for early CRC diagnostics (17–21).

The RNA binding protein insulin-like growth factor 2 mRNA binding protein 1 (IGF2BP1/IMP1) is emerging as a potential regulator of EV biology (22–24). Although IMP1 is highly expressed in CRC (25, 26) and is associated with poor prognosis (26, 27), its role in CRC EV biology is unknown. As an RNA binding protein, IMP1 binds to mRNA target transcripts and regulates their stability, localization, and translation (28–32). IMP1 binding is dependent upon target nucleotide sequences (22, 23, 33) and/or N^6-methyladenosine (m6A) marks (29), which is a dynamic, temporal, and tissue-specific modification that facilitates interaction with RBPs and subsequent modulation of gene expression and mRNA transcript stability (29, 34–36). IMP1 binds and stabilizes numerous transcripts with known roles in CRC, including *KRAS* (37), *cMYC* (38, 39), *CD44* (40), *PTGS2* (41), *MDR1* (42), *ITGB5* (22), as well as many other mRNAs that could serve as biomarkers of this cancer (28).

In this study, we used human CRC in vitro and in vivo models to test whether IMP1 expression levels impact human CRC cell-dependent EV synthesis, secretion, and/or cargo.

METHODS

Cell Lines

Parental cell lines (Caco2, SW480, and HT-29) were obtained from the American Type Tissue Culture Collection (ATCC, Manassas, VA). The ATCC authenticates all human cell lines through short tandem repeat analysis. All cell lines were confirmed to be mycoplasma negative every 3 wk (MycoAlert Mycoplasma Detection Kit, Lonza, Bend, OR). IMP1 was knocked out in HT-29 and SW480 cells using CRISPR/Cas9 and FLAG-IMP1 was overexpressed as described by Andres et al. (43). All cell lines were maintained in DMEM-H (Gibco, Thermo Fisher, Waltham, MA), 10% FBS (Cytiva, Marlborough, MA), and 1% penicillin-streptomycin (Gibco). HT-29 and SW480 cell lines expressing FLAG-IMP1 were maintained with 2 μg/mL puromycin (Goldbio, St. Louis, MO), as described by Andres et al. (43). All cell counting was performed using the Countess 3 automated cell counter (Thermo Fisher) and Trypan blue staining to differentiate between live and dead cells. Cell viability was assessed in EV secretion experiments.

Colonoid Culture

Colonoid lines were generated from mice expressing FLAG-tagged Imp1 in an intestinal and colonic-epithelial specific manner ($Imp1^{OE}$) based on expression of Villin-Cre (44). Colonoids were generated from $Imp1^{OE}$ and Imp1 wild-type (WT) mice as described by Mizutani and Clevers (45) with the following modifications. Colon tissue was harvested, flushed with PBS, longitudinally opened, and cut into 5-mm tissue pieces. Tissue pieces were then washed with PBS 15 times before transfer to colonic crypt isolation buffer (5×: Na_2HPO_4, 28 mM; KH_2PO_4, 40 mM; NaCl, 480 mM; KCl, 8 mM; sucrose, 220 mM; D-sorbitol, 274 mM) for 20 min at room temperature to lift crypts (one fraction). Fractions 3, 4, and 5 were used downstream. Fractions containing crypts were centrifuged at 290 *g* for 5 min at 4°C. Pellet was resuspended in 4 mL of cold DMEM/F12 at 200 *g* for 3 min at 4°C. Colon crypts were resuspended in 3:2 Matrigel (MG):basal media [basal media: 1% penicillin/streptomycin (Gibco, Waltham, MA), 10 mM HEPES (Thermo Fisher, Waltham, MA), 1× Glutamax (Fisher Scientific, Pittsburgh, PA)] for plating. For experimental setup, colonoids were dissociated with cell recovery solution (Corning, Corning, NY), centrifuged at 300 *g* for 5 min, resuspended in 3:2 Matrigel:basal media.

For each experiment, 200–300 colonoids/well were plated in Matrigel (MG) patties in 4 wells per colonoid line. MG patties were polymerized for 15 min at 37°C before 500 μL of mouse Intesticult (STEMCELL Technologies, Vancouver, Canada), with 1% penicillin-streptomycin (Gibco) and 0.25 μg/mL amphotericin B (Sigma, St. Louis, MO) was added. Bright-field images were taken using a Keyence BZ-X800 (Keyence, Itasca, IL) with a ×2 objective, 0.1 numerical aperture (NA).

RNA Sequencing

HT-29 null and $IMP1^{OE}$ tumor-derived cell lines (n = 2 passages/genotype) were grown and RNA-seq libraries were prepared as described previously by Chatterji et al. (44).

RNA Sequencing Analysis

Adapters were removed and raw reads were simultaneously demultiplexed from a single library using cutadapt (46). Trimmed reads were aligned using kallisto (47) against a reference transcriptome based on Gencode release 39, which contained a single, primary transcript isoform for each gene. Primary isoforms of genes were determined using the APPRIS database (48). Differential expression was performed using DESeq2 (49). A gene was considered differentially expressed if it had both a q value $\leq$0.05 and at least a log2-fold change = 0.5. A complete list of genes is shown in GSE198804. Gene ontology (GO) analysis (50, 51) was conducted using the online GO enrichment tool (52). Specifically, IDs for all significant genes were used to search the GO Cellular Compartment ontology using the statistical overrepresentation test and Fisher's exact test options. Data processing and analysis was performed using the R programming language (53). Source data files are deposited in GEO and can be accessed at GSE198804.

Xenograft Studies for Circulating Extracellular Vesicle Isolation

All animal studies were performed in accordance with University of Pennsylvania IACUC (Protocol No. 805829) guidelines. Female, NCr nude mice aged 8 wk (CrTac:NCr-Foxn1nu; Taconic, Germantown, NY) were anesthetized with isoflurane (1.5%–4%) before injection of 1×10^6 cells (HT-29 null or HT-29 IMP1^{OE}) in 100 μL of 50:50 Matrigel and Dulbecco's modified Eagle's medium (DMEM)-high glucose in the left and right flank. Animals were maintained with ad libitum access to food and water and on a 12-h light/dark cycle. Tumor volume was measured weekly using calipers and tumor mass was measured following tissue harvest. Animals were euthanized by carbon dioxide asphyxiation when total tumor volume was approximately 500 mm^3 or ulceration necessitated euthanasia. After euthanasia, whole blood was collected by cardiac puncture into ETDA-coated tubes and final tumor volume and mass were recorded. Data presented are from n = 5 untreated and n = 9 null or IMP1^{OE} tumor-bearing animals. Animals treated with topical antibiotics were excluded from the study.

Nanoscale Flow Cytometry of Human Colorectal Cancer Extracellular Vesicles

Fresh blood was collected in EDTA tubes from these mice and centrifuged at 2,500 g for 15 min (Sorvall ST16R, brake on medium low) to generate platelet poor plasma, which was dispensed into 50-μL aliquots, flash frozen, and banked at −80°C. Importantly, all blood samples were uniformly collected, centrifuged within 2 h, and banked at −80 for batch testing. Anti-human EpCAM APC-cy7 (Abcore) and CD63-PEcy7 (BD Biosciences) optimal dilutions (0.2–0.02 μg/mL) were determined by testing dilution series in positive and negative control samples (human pancreatic cancer culture media and mouse plasma from animals lacking human tumor implantation). Negative controls also included monoclonal isotypes, antibody-stained 0.1 μm PBS, and EV-depleted mouse plasma that were treated overnight with 5% DMSO at room temperature. Plasma samples were stained for 1 h at room temperature then diluted 1:300 into "200 nm bead buffer" (Polysciences.com), which was made by nanoFACS sorting 200 nm polystyrene beads into 0.1-μm filtered PBS. Bead buffer of 200 nm provided both a "relative" internal size standard and a means to standardize the volume of stained plasma tested (e.g., 1,000 beads equaled 1 μL of starting plasma tested on our BD Biosciences FacsAria Fusion). Nanoscale flow cytometry imaging and counting of stained EVs was performed as described by our group and others (54–56). Briefly, the approach used the combination of both side light scatter (SSC-H) reported on the log scale of the y-axis and antibody-fluorophore labeling reported on the x-axis, which distinguished relative EV sizes (compared with commercially available polystyrene bead standards ranging in size from 100 nm to 900 nm, *Megamix-Plus FSC and -Plus SSC, BioCytex*) and multiplex antibody target specificity (only EpCAM+/CD63+ events were counted). Labeled EVs were distinguished from the unlabeled nanoparticle "noise" of similar size (e.g., lipoproteins, nonspecific cell fragments) by positive antibody staining fluorescent signal. Fluidic and instrument settings were designed to minimize background noise while maximizing the detection of submicron-sized EVs. SSC-H voltage was uniformly adjusted for all experiments so 200-nm beads were at 10^4 and 900-nm beads remained on the visible log x-scale. All flow machine buffers were filtered with a ZenPure PureFlow Mini Capsule PES 0.1-μm filter. Imaging was performed on a FacsAria Fusion (BD Biosciences) with a 70-μm nozzle and 0.1-μm filtered PBS sheath fluid at a pressure of 70 psi. Settings were considered adequate if 0.1-μm filtered PBS generated "noise" at fewer than 1,000 events per second. Coincident EV events per nanoliter droplet were controlled by using a threshold rate of <40,000 events per second and electronic abort rate <5%. An essential criterion for reproducibility was setting uniform gates in advance of batch analysis with positive and negative control plasma samples. All samples used the same preset gates defined relative to MegaMix beads, MESF beads (BD Biosciences), and plasma controls. Data were collected based on uniform 200 nm bead dilution buffer for each sample and reported as gated events per microliter of starting plasma. The mean of triplicate experiments for each sample was used for statistical analysis of EpCAM+/CD63+-positive colabeled EV events. Data are presented as the mean and SE from n = 5 untreated and n = 9 null or IMP1^{OE} tumor-bearing animals and compared using one-way ANOVA or Student's t test with $P < 0.05$ being considered statistically significant.

Extracellular Vesicle-Depleted FBS

Extracellular vesicles (EVs) were depleted from FBS (Cytiva) using a 400-mL Amicon Stirred Cell (MilliporeSigma, Burlington, MA) with Biomax 300-kDa Ultrafiltration Disks (MilliporeSigma) for 4–6 h. Supernatant was used for making EV-depleted DMEM in subsequent experiments. EV depletion was assessed by running the cell culture media containing filtered FBS on ZetaView Quatt Nanoparticle Tracking Analyzer (Particle Metrix) (Supplemental Fig. S1; all Supplemental material is available at https://doi.org/10.6084/m9.figshare.c.5983702.v1).

Extracellular Vesicle Isolation by Size-Exclusion Chromatography—Cell Lines

For EV secretion experiments, 1 million HT-29 or SW480 cells with and without IMP1 expression were plated and allowed to attach to a 10-cm dish overnight. For EV cargo experiments, 2.5 million cells were plated and allowed to attach to a 15-cm dish overnight. The next day, the cells were washed once with warm 0.1-μm filtered PBS (Gibco). Cells were then incubated overnight in DMEM-H (Gibco) containing EV-depleted FBS (EVD-FBS; final concentration = 10%); 1% penicillin-streptomycin (Gibco). EV-conditioned media containing secreted EVs was collected after 48 h. Media was centrifuged at 386 g for 10 min. Supernatant was concentrated down to <200 μL with passivated Amicon Ultra-15 Centrifugal Filter Units (MilliporeSigma) at 5,000 g (time is dependent on the initial volume). EVs were then isolated using a qEV single column (IZON Science, Christchurch, New Zealand) following manufacturer instructions. Briefly, 200 μL fractions were collected into 1.5-mL Protein LoBind Microcentrifuge Tubes (Eppendorf, Hamburg, Germany).

The presence of EVs in *fractions 7* and *8* were verified by Western blot analysis for CD9 (Supplemental Fig. S2). Equal volume of sample was concentrated by boiling and loaded for *fractions* 3–11 (due to low protein measurement) and 15 μg of protein was loaded for *fractions 12–15*. Protein concentration was quantified using Nanodrop 2000c (Thermo Fisher Scientific).

Extracellular Vesicle Isolation by Size-Exclusion Chromatography—Colonoids

Forty-eight hours postseeding, colonoid media was replaced with fresh complete Intesticult (STEMCELL Technologies). Conditioned media was harvested twice: first at 48 h and again 72 h later and then centrifuged at 10,000 *g* for 20 min at 4°C to get rid of debris. Collected conditioned media was concentrated down to <150 μL with passivated Amicon Ultra-2 Centrifugal Filter Units (MilliporeSigma) per instructions. Briefly, conditioned media was loaded and centrifuged at 3,000 *g* for 10-min intervals at 15°C. EVs were then extracted using qEV single columns (IZON Science) as with human CRC cell media. EV-enriched fractions were then collected (~400 μL) and concentrated down to <50 μL with a SpeedVac (Thermo, DNA-120). Protein concentration was quantified using microBCA kit (Pierce, Thermo Scientific).

Nanoparticle Tracking Analysis

Nanoparticle tracking analysis was performed using Zetaview Quatt (Particle Metrix, Inning am Ammersee, Germany) to quantify particles using di8 lipid membrane dye (Thermo Fisher). Di8, at a concentration of 1:1,000, was incubated with the EV samples for 15 min in the dark. For all samples data were acquired and averaged over 11 image positions at a temperature of 25°C. For samples isolated from cell lines and stained with Di8, data were collected at an intensity of 80, gain = 38.4. All samples were diluted in 0.1-μm filtered PBS, which contained minimal particles and fell below the level of detection on the ZetaView. Each sample was run in triplicate and values shown are the average of triplicate runs performed on $n = 3$ independent passages of each cell line. Each run included the saline used for sample dilution and fresh media containing all treatments or additives to confirm low levels of background particles.

Protein Isolation, Quantification, and Western Blotting

Cells were lysed in RIPA lysis buffer [20 mM Tris·HCl (Fisher Scientific); 100 mM KCl (Thermo Fisher); 5 mM $MgCl_2$ (Fisher Scientific); 1 mM DTT (Fisher Scientific); 0.5% TritonX-100 (Fisher Scientific) with fresh phosphatase inhibitor cocktail] or 1× radioimmunoprecipitation assay (RIPA)-SDS [Cell Signaling Technology (CST), Danvers, MA] with protease and phosphatase inhibitors (Thermo Fisher). Protein concentration was determined by bicinchoninic acid (BCA) assay (Thermo Fisher) following manufacturer instructions. For whole cell lysates, equal protein concentrations were run on 4%–12% bis-tris gels (Thermo Fisher) and transferred to 0.45-μm nitrocellulose or PVDF membrane. EVs were lysed in 6× SDS/laemmli, concentrated by evaporation (cell lines) and/or loaded in equal microgram amounts as indicated, run on a 4%–12% bis-tris gel (Thermo Fisher), and transferred to PVDF membrane (Immobilon, Millipore/Merck). The membrane was blocked in LI-COR blocking buffer (LI-COR, Lincoln, NE) or 5% BSA (Goldbio) in PBS (Fisher Scientific). Primary antibodies were as follows: anti-Alix (Santa Cruz, sc-53540, 1:5,000); anti-CD63 (System Biosciences, Palo Alto, CA, EXOAB-CD63A-1, 1:1,000) or for whole cell lysate (WCL; Abcam, ab134045, 1:1,000); anti-CD9 (System Biosciences, EXOAB-CD9A-1, 1:1,000); anti-GM130 (Novus Biologicals, Littleton, CO, NBP2-53420, 1:1,000); anti-TSG101 (BD Biosciences 612696; 1:1,000); anti-GAPDH Mab374 [Chemicon (Fisher Scientific); 1:10,000]; anti-FLAG M2 (Sigma/Millipore/Merck, F1804; 1:5,000); anti-IMP1 (MBL International, Woburn, MA, RN007P; 1:1,000); anti-IMP1 (Cell Signaling Technology, Danvers, MA, CST2852, 1:1,000); Rab27A (00045, 1:500). Secondary antibodies were: anti-mouse-HRP and anti-rabbit HRP (CST; 1:10,000), anti-mouse 680/800, anti-rabbit 680/800 (LICOR, 1:15,000) depending on the imaging platform. PVDF membranes with fluorescent secondary antibodies were imaged on LICOR Odyssey. Nitrocellulose membranes with HRP-conjugated secondary antibodies were overlaid with ECL ultra (Pierce, Thermo Fisher). The specificity of the MBL anti-IMP1 antibody was confirmed by a competitive protein binding assay using recombinant IMP1 protein (RayBioTech, Peachtree Corners, GA). Densitometry analysis was performed using the area under the curve function with ImageJ v.2.1.0 or the image analysis function on LI-COR Image Studio Lite v.5.2.5.

Immunofluorescence

HT-29 cells were seeded on coverslips at a low density and allowed to attach overnight. The next day cells were fixed in 4% paraformaldehyde (PFA, Fisher Scientific) for 20 min. Fixed cells were washed three times with 1× PBS. Cells were permeabilized in 0.1% Triton-X 100 (Fisher Scientific) in PBS for 10 min, followed by three washes with PBS. Permeabilized cells were then blocked with 5% BSA (Sigma) in PBS for 30 min. Primary antibody to CD63 was diluted in blocking solution as follows: anti-CD63 (mouse; Abcam, Cambridge, UK; ab8219; 1:200) and incubated overnight at 4°C. The next morning, coverslips were washed three times with 1× PBS before 1-h incubation with secondary antibody. Secondary antibody was diluted 1:500 in blocking buffer anti-mouse-488 (Invitrogen). After secondary, nuclei were stained with DAPI (1:10,000 in PBS) for 5 min. Coverslips were washed three times with PBS and mounted on slides using VectaShield mounting media (Vector Labs, Burlingame, CA). Unless indicated, all steps were carried out at room temperature. Images of CD63 were taken using a Nikon confocal microscope with a ×100 oil immersion objective, 1.45 NA with an Andor iXon3 EMCCD camera (Oxford Instruments, Abingdon, UK) using NIS-Elements AR software (Nikon, Tokyo, Japan).

Transmission Electron Microscopy on Cell Pellets

Transmission electron microscopy (TEM) was performed on fixed cell pellets from null and $IMP1^{OE}$ HT-29 cells using conventional methods. TEM micrographs were collected using Tecnai T12 TEM microscope operating at 100 keV and the images were recorded at ×20 mag on Gatan 4K CMOS camera.

Immuno-Electron Microscopy

Fixed extracellular vesicles isolated from SW480 null and IMP1^{OE} cell-conditioned media were placed on formvar-coated 200 mesh copper grids for 5 min. Residual aldehydes were quenched in 0.15% glycine in 1× PBS. The extracellular vesicles were then permeabilized with 0.01% Triton X-100 in 1× PBS for 5 min, rinsed in 1× PBS, and then blocked with 1% BSA and 0.1% fish skin gelatin in 1× PBS for 15 min. The extracellular vesicles were immunolabeled with mouse anti-FLAG primary antibody (F1804, Sigma Aldrich) diluted 1:20 in blocking buffer for 1 h, rinsed in 1× PBS, labeled with goat anti-mouse 15 nm gold secondary antibody (Cat. No. 25133, Electron Microscopy Sciences) diluted 1:20 in blocking buffer for 30 min and rinsed in 1× PBS. The small EVs were then fixed with 1% glutaraldehyde in 1× PBS for 5 min, rinsed in water, and stained with 2% uranyl acetate for 5 min. All incubation steps were performed at room temperature. Samples were imaged at 120 kV on a FEI Tecnai Spirit TEM system. Images were acquired using the AMT interface on an AMT 12 Megapixel NanoSprint12S-B cMOS camera system.

RNA Isolation and qRT-PCR from EVs

RNA was extracted from 200 μL of size-exclusion chromatography (SEC)-isolated EV suspension from cell culture conditioned media by using the MagMAX mirVana Total RNA Isolation Kit (Thermo Fisher). The manufacturer protocol for isolating RNA from urine samples was used. Total Lysis Binding Mix was modified to account for reduced sample input: for 200 μL of sample, 158.4 μL lysis buffer and 1.6 μL 2-mercaptoethanol. SuperScript IV VILO Master Mix (Invitrogen, Waltham, MA) was used for cDNA synthesis, following manufacturer instructions. Applied Biosystems TaqMan Fast Advanced Master Mix (Thermo Fisher) was used for RT-qPCR on StepOnePlus Real-Time PCR System Applied Biosystems (Thermo Fisher). Taqman with Gene Expression Assays *KRAS* (Hs00364282_m), *MYC* (Hs00153408_m1), *ITGB5* (Hs00174439_m1), *MDR1* (Hs00184500_m1 *ABCB1*), and *PTGS2* (Hs00153133_m1) were used. n = 3 independent samples were run in duplicate for each group. Data were analyzed using the ddCT method and normalized to the housekeeping gene *OAZ1* (Hs00427923_m1).

Statistical Analyses

All values are presented as the means ± SE. The significance was determined with an unpaired t test or one-way ANOVA with multiple comparisons and Tukey's test calculated using GraphPad Prism 9.0, depending on the data set analyzed as indicated in the figure legend. A P value <0.05 was considered significant.

RESULTS

We utilized two CRC cell lines, HT-29 and SW480 in which endogenous IMP1 was deleted by CRISPR and then FLAG-IMP1 with a short 3′ untranslated region was re-expressed to ensure minimal miRNA regulation and high levels of IMP1 expression (Fig. 1*A*) (43). To evaluate IMP1-mediated molecular changes in RNA expression in CRC cells, we performed RNA sequencing in HT-29 null and IMP1^{OE} cells. HT-29 cells were selected since they do not express endogenous IMP1 and are capable of differentiation (43, 57).

IMP1 Alters Gene Expression in Exosome and Extracellular Vesicle Pathways

Differentially expressed transcripts that were significantly changed relative to IMP1 expression were compared using GO analysis (Tables 1 and 2). The extracellular exosome and extracellular vesicle pathways were among the top four most significantly differentially regulated pathways in the IMP1-expressing cells and the vesicle pathway was in the top seven (Table 1). Pathways involved in protein synthesis regulation, including ribosomal subunits, were among the most changed pathways (Table 2). Over 30% of significantly altered transcripts were associated with exosome biogenesis, regulation, or cargo (Fig. 1*B*). We assessed expected changes in gene expression and found *IGF2* highly upregulated and *GDF15* to be downregulated in IMP1-expressing cells (Fig. 1*C*; Supplemental Table S1) (58, 59). IMP1 induced a modest upregulation in genes with the potential to influence EV biogenesis, cargo loading, or previously found within EVs (60–66), including *AQP5, TUBB, YWHAQ, HSPA8, SERPINA1,* or *MSN* (Fig. 1*C*; Supplemental Table S2) (all genes selected based on $q \leq 0.05$ and log2-fold change $\geq$ 0.5). These data indicate potential roles for IMP1 in modulating EV production or cargo. MSN was recently identified as a novel EV marker in a study of over 400 human samples from a variety of tissue and biofluid sources (61). Notably, in a small study of n = 36 patients, SERPINA1 was upregulated in the circulating EVs isolated from patients with CRC compared with healthy controls (63).

IMP1 Does Not Alter EV Secretion In Vitro

Our pathway analyses suggest roles for IMP1 in modulating EV pathways, therefore, we examined if IMP1 expression could affect EV secretion in CRC cells. We used IMP1 null and IMP1^{OE} HT-29 and SW480 CRC cell lines (Fig. 2*A*) and examined expression of proteins known to be involved in EV biogenesis and/or secretion, including accessory protein ALIX, tetraspanin CD63, which are commonly secreted within EVs (67), and Rab27A, which is important for EV secretion (68). Interestingly, we found no significant differences in the amount of protein expression with respect to IMP1 across n = 3 passages of each cell line (Fig. 2*A*; Supplemental Fig. S3*A*). To further characterize the effects of IMP1 on vesicle formation, we assessed multivesicular bodies (MVB) marked by CD63 by immunofluorescence and intraluminal vesicles using transmission electron microscopy. We found that IMP1^{OE} and null cells contain numerous, CD63-positive MVB (Fig. 2*B*) that were often packed with vesicles (Fig. 2*C*).

Although we did not observe major differences in the expression levels of select EV biogenesis or secretion proteins, we next assessed whether IMP1 expression had a functional impact on the number of EVs that were secreted from CRC cells. We used size-exclusion chromatography (SEC) to isolate EVs from the conditioned media of HT-29 and SW480 null and IMP1^{OE} cells. We used Nanoparticle Tracking Analysis (NTA) coupled with a lipid membrane dye (Di8) to quantify the size and number of the isolated

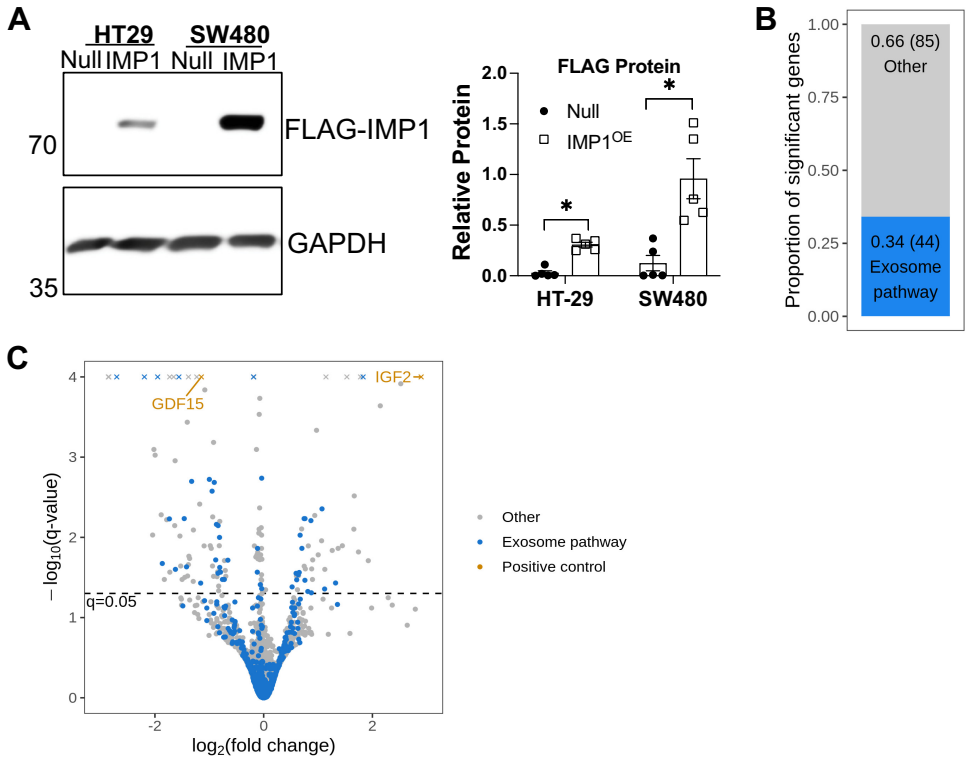

Figure 1. IMP1 is associated with transcript level changes in exosome and extracellular vesicle pathways. *A*: Western blot analysis for FLAG protein confirms CRISPR deletion of endogenous IMP1 in null/empty vector control cell lines and overexpression of FLAG-tagged IMP1 via Piggybac vector in IMP1-overexpressing lines (IMP1^{OE}). Blot represents $n = 5$ independent passages. Relative FLAG-IMP1 protein expression was normalized to loading control GAPDH and quantified using densitometry, shown in the bar graph. Densitometry was performed using the area under the curve function with ImageJ v.2.1.0 or the image analysis function on LI-COR Image Studio Lite v.5.2.5. $P < 0.05$ versus null control by unpaired *t* test. Total RNA was isolated from null and IMP1-overexpressing HT-29 cell lines, $n = 2$ independent cell lines per genotype for RNA sequencing. There was a highly significant and strong correlation between the null control and IMP1^{OE} replicates (see Supplemental Fig. S5*A*). IMP1 expression resulted in modest up- and downregulation of gene expression (see Supplemental Fig. S5*B*). *B*: over 30% of all differentially expressed genes were associated with extracellular vesicle pathways. *C*: individual genes are shown in the volcano plot, created in R where all genes are shown by their log2-fold change and false discovery rate-adjusted *P* value. Genes that are members of the GO exosome pathway are shown in blue. The two positive controls, IGF2 and GDF15, are shown in gold. Circular points indicate true adjusted *P* value while X points are artificially lowered to aid in visualization. X points are more significant than indicated. The full results are available in Supplemental Table S3.

vesicles. Consistent with our molecular data, we found that IMP1 expression did not alter EV secretion from HT-29 or SW480 CRC cell lines (Fig. 2*D*). Importantly, there were no significant differences in total cell number (Fig. 2*E*) or viability (Fig. 2*F*) at the time of media harvest. We confirmed EV identity following the MISEV 2018 guidelines (13) and demonstrated that the isolated EVs contain CD63, TSG101, CD9 and were negative for the Golgi protein GM130 (Fig. 2*G*; Supplemental Fig. S3*B*). Together this body of evidence indicates that IMP1 does not alter in vitro EV secretion.

Table 1. *Most significantly differentially regulated pathways*

Term	Fold Enrichment	*P* Value	FDR
Extracellular membrane-bounded organelle	3.05	9.89e-26	6.68e-23
Extracellular exosome	3.05	1.66e-25	8.39e-23
Extracellular organelle	3.05	9.89e-26	1.00e-22
Extracellular vesicle	3.05	9.54e-26	1.93e-22
Extracellular space	2.26	1.02e-19	4.12e-17
Extracellular region	2.02	9.22e-19	3.12e-16
Vesicle	2.05	4.21e-17	1.22e-14
Cytoplasm	1.36	2.28e-15	5.77e-13
Intracellular anatomical structure	1.21	2.70e-11	6.09e-09
Cytosol	1.63	8.45e-11	1.71e-08

FDR, false discovery rate.

IMP1 Does Not Alter In Vivo EV Secretion

Cancer cells continually communicate with and are shaped by their surrounding microenvironment. EVs are one critical mediator of this information flow (69). To evaluate whether IMP1 expression alters EV secretion in vivo in the presence of mesenchymal cell types, we performed subcutaneous xenografts using HT-29 IMP1 null and IMP1^{OE} cells. Platelet poor plasma was collected when total tumor volume reached ~500 mm^3 or ulceration necessitated euthanasia. We then performed nanoscale flow cytometry (controls and validation shown in Supplemental Fig. S4) to assess the size and number of human CD63/EpCAM+ EVs secreted from the HT-29 tumors into the mouse circulation (Fig. 3*A*). We found that circulating CD63+/EpCAM+ EVs were increased in some tumor-bearing mice, but there was no correlation with IMP1 expression levels (Fig. 3*B*). Notably, the mean tumor volume was not significantly different between groups (353 mm^3 and 382 mm^3 in null versus IMP1^{OE} tumor-

Table 2. *Most changed pathways*

Term	Fold Enrichment	*P* Value	FDR
MHC class I protein complex	27.15	4.21e-05	0.00328
Microvillus membrane	14.1	1.06e-05	0.0012
Mitochondrial respiratory chain complex IV	10.63	8.65e-04	0.0337
MHC protein complex	9.4	0.0013	0.0439
Respiratory chain complex IV	9.4	0.0013	0.0432
Cytosolic small ribosomal subunit	8.33	1.46e-04	0.0074
Cytosolic ribosome	7.71	4.83e-08	7.53e-06
Cytosolic large ribosomal subunit	7.37	8.25e-05	0.00492
Microvillus	6.11	3.18e-05	0.00258
Lysosomal lumen	5.67	5.46e-05	0.00395

FDR, false discovery rate; MHC, major histocompatibility complex.

injected animals, respectively) (Fig. 3*C*). These data suggest that IMP1 does not alter human CRC EV secretion in vivo.

IMP1 Enters EVs In Vitro

Given known and emerging roles for RNA binding proteins in regulating EV cargo (23), we next asked whether IMP1 directly or indirectly alters EV cargo using a panel of CRC cell lines (Fig. 4*A*). We included Caco2 cells, which express high levels of endogenous IMP1, 78-fold more than our HT-29 $IMP1^{OE}$ cells; wild-type (WT) SW480 cells that express moderate-high levels of endogenous IMP1, 31-fold more than HT-29 $IMP1^{OE}$ cells; as well as HT-29 and SW480 $IMP1^{null}$ and $IMP1^{OE}$ cells. These additional wild-type cell lines were included to control for any potential artifacts of the FLAG-IMP1 protein.

EVs were isolated from an equal volume of culture media derived from plating of equal numbers of cells across all lines by SEC. EV identity was confirmed by Western blot analysis using CD9 (Fig. 4*B*). We found that IMP1 enters the EV in WT and $IMP1^{OE}$ SW480 cells, as well as Caco2 cells but not in HT-29 $IMP1^{OE}$ cells (Fig. 4*B*). We further confirmed the presence of FLAG-IMP1 in EVs isolated from SW480 $IMP1^{OE}$ cells by Western blot (Fig. 4*C*) and immunoelectron microscopy for FLAG protein (Fig. 4*D*). The specificity of CD9 to SEC *fractions 7–8* is illustrated in the full blot from this experiment in Supplemental Fig. S2.

To examine if IMP1 directly alters EV RNA cargo, we performed targeted qPCR to examine expression levels of known IMP1 binding targets. We isolated RNA from EVs secreted by IMP1 null versus $IMP1^{OE}$ SW480 cells and assessed the expression of *KRAS* (37), *MYC* (38, 39), *ITGB5* (22), *PTGS2* (41), and *MDR1* (42) by qPCR (Fig. 4*E*). We found packaging of *KRAS*, *MYC*, *ITGB5*, and *MDR1* transcripts into CRC cell EVs, whereas *PTGS2* was generally absent. We did not detect a significant difference in the amount of these transcripts with respect to IMP1. This could be due to redundancy of RNA binding proteins that traffic into CRC EVs, such as Ago2 (52, 71) or indicative of IMP1 not transporting these particular transcripts in this context. In summary, these data indicate the IMP1 enters the EV in select CRC cell lines, but that it does not alter levels of well-recognized IMP1 targets including, *KRAS, MYC, ITGB5,* or *MDR1* transcripts.

IMP1 Does Not Enhance Vesicle Secretion from Nontransformed Colonoids

Since IMP1 is highly expressed during and critical to gut development (72), we next asked if high levels of IMP1 would affect EV secretion or cargo in the nontransformed colonic epithelium. To address this, we utilized mouse colonoid cultures derived from the colon of mice expressing Imp1 in an intestinal and colonic epithelial specific manner ($Imp1^{OE}$) based on expression of Villin-Cre (44) (Fig. 5*A*).

We isolated EVs secreted by colonoids from $Imp1^{OE}$ and Imp1 wild-type (WT) mice (Fig. 5*B*). We confirmed EV identity by Western blot analysis for CD9, a protein considered to mark EVs, based on MISEV 2018 guidelines (13) (Fig. 5*C*). Interestingly, despite elevated levels of Imp1 expression, we did not detect Imp1 in EVs secreted from nontransformed colonoids (Fig. 5*C*), suggesting that IMP1 entry into the EV maybe specific to CRC cells. However, this does not eliminate the possibility that Imp1 indirectly alters EV cargo by changing RNA or protein expression within the colonoids themselves.

Taken together, these data suggest that although IMP1 influences the RNA expression of transcripts from extracellular vesicle pathways, IMP1 expression in CRC cell lines does not have observable effects on EV secretion in vitro or in vivo. IMP1 does however influence EV cargo in CRC by entering EVs from CRC cell lines with high IMP1 expression (Fig. 6). This suggests that IMP1 could be a useful biomarker for indicating primary tumor IMP1 status, if circulating IMP1 can be detected in human patients.

DISCUSSION

Increased IMP1 expression is observed in 70% of CRC tumors; and, overexpression of IMP1 is associated with increased tumor stage and poor prognosis (26, 27). IMP1 is known to influence numerous signaling pathways, including KRAS (37, 73), cMYC (38, 39, 74, 75), and WNT (39, 40, 44, 74–77) that could affect EV secretion (78–80) and/or cargo loading (71, 81–84), but the relationship between IMP1 and CRC EV biology remained to be explored.

In this study, we demonstrate that IMP1 enters CRC EVs in SW480 and Caco2 human cell lines where it may directly alter EV RNA cargo. Despite significant potential to alter EV production or secretion, we observed no changes in the number of EVs secreted from CRC cells in vitro or in vivo related to IMP1 expression levels.

RNA sequencing data suggested that increasing IMP1 levels alters transcripts known to regulate EV pathways, but we did not observe differences in CRC EV secretion. Perhaps this is due to changes that both up- and downregulate EV regulation pathways, resulting in a net neutral change. Alternatively, changes in expression could be related to the

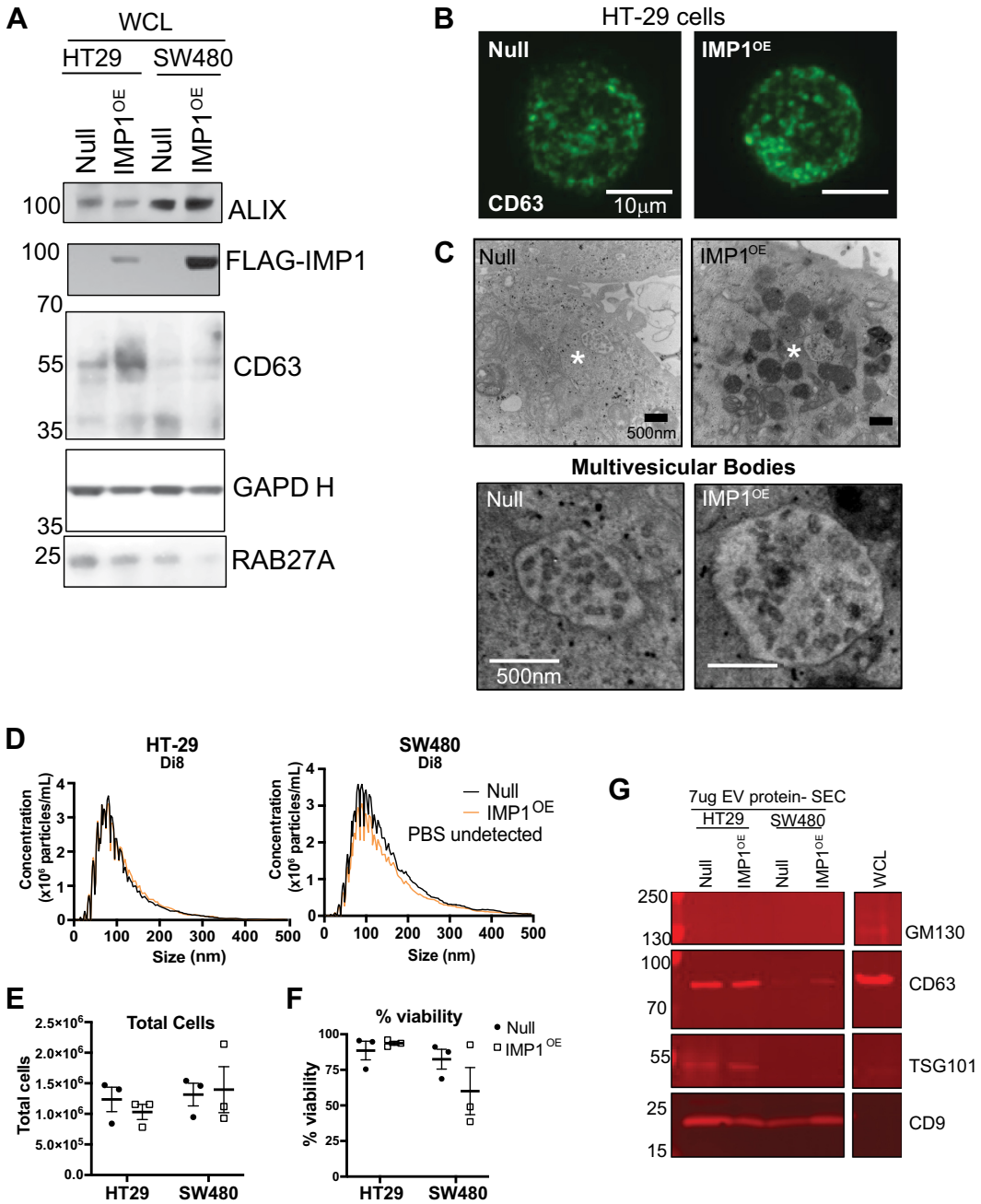

Figure 2. IMP1 has little effect on in vitro extracellular vesicle (EV) secretion in colorectal cancer cells. *A*: effects of IMP1 expression on protein levels of extracellular vesicle (EV) markers and EV biogenesis proteins were assessed by Western blot in whole cell lysate (WCL) from HT-29 and SW480 null vs. IMP1^{OE} cell lines. Blots were performed on n = 3 independent passages of each cell line. Densitometry is shown in Supplemental Figure S3*A*. Densitometry was performed using the area under the curve function with ImageJ v.2.1.0. *B*: multivesicular bodies (MVB) were evaluated using CD63 immunofluorescence in HT-29 cells. A representative image from *n* = 3 passages is shown. Scale bar = 10 μm. *C*: MVB size and vesicle density were assessed by transmission electron microscopy using pellets of HT-29 null and IMP1^{OE} cells. *D*: EV secretion was examined by nanoparticle tracking analysis via Di8 lipid membrane staining on a ZetaView Quattro. Samples were isolated by size-exclusion chromatography (SEC) from conditioned media collected from HT-29 and SW480 null versus IMP1^{OE} cell lines after 48 h of culture. Data shown are the average of Nanoparticle Tracking Analysis (NTA) run in triplicate on *n* = 3 independent passages of cells. There was no difference in total cell number (*E*) or cell viability (*F*) at the time the conditioned media was isolated. EV identity was assessed by Western blot using protein isolated from the SEC EV preparation (*G*) and markers (CD63, TSG101, CD9, and Golgi marker GM130) described in MISEV 2018 (13). Densitometry values were calculated using Licor Image Studio Lite v5.2.5 and are shown in Supplemental Figure S3*B*.

effects of IMP1 on the autophagy pathway (85), which is interconnected with EV pathway regulation (86–95). It is also possible that IMP1 alters secretion or production of larger microvesicles. This study focused exclusively on smaller EVs and excluded microvesicles larger than 1 μm from our preps via centrifugation. In turn, future studies might focus on larger microvesicles or oncosomes to see if IMP1 modulates their secretion. It is unlikely that differences

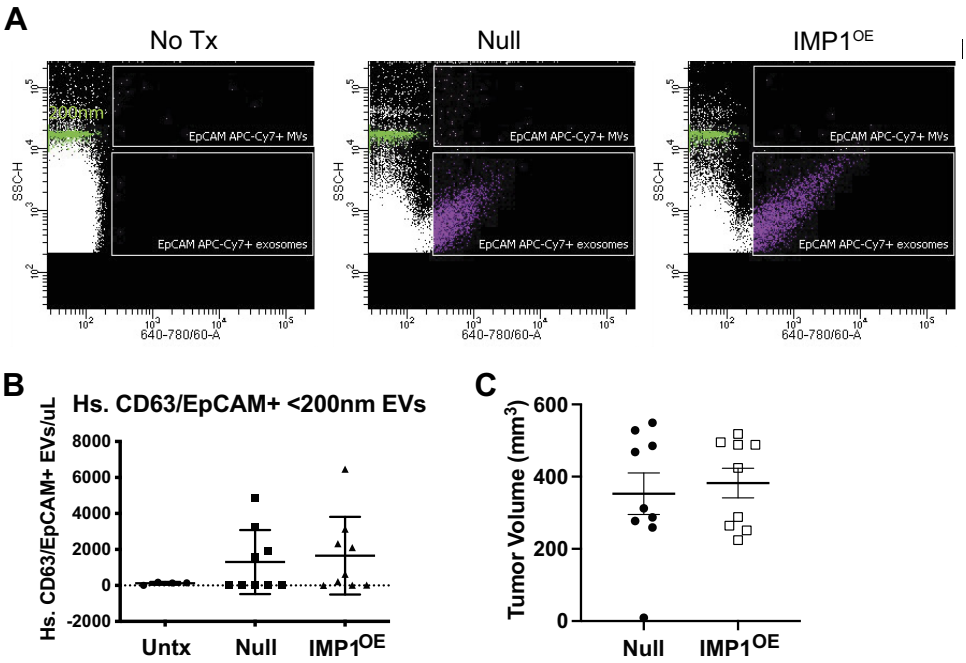

Figure 3. IMP1 does not alter circulating extracellular vesicle (EV) number in vivo. *A*: representative nanoscale flow cytometry plots for human EpCAM + /CD63 + vesicles in the platelet-poor plasma isolated from xenograft mice untreated (untx), or injected with HT-29 IMP1^{null}, or HT-29 IMP1^{OE} cells. *B*: average number of circulating EpCAM + /CD63 + EVs were quantified using the mean of triplicate experiments and reported as counts/μL of plasma. *C*: average tumor volume was determined using calipers and the following equation (width × width × length/2) where width is the smaller and length is the larger of the two dimensions measured. Each dot represents a single animal. Untx, animals were not injected with human colorectal cancer (CRC) tumor cells. Error bars represent means ± SE. n = 4 untx, n = 9 null, n = 9 IMP1^{OE} xenograft animals.

in EV secretion may be masked by the elevated level of EV production by CRC cells, since high levels of IMP1 also do not alter EV secretion in our nontransformed colonoids. Our current working hypothesis is now that IMP1 function in CRC EV biology may be focused on EV cargo.

We observed that IMP1 enters EVs from SW480 and Caco2 cells lines but not in HT-29 cell lines or colonoids overexpressing IMP1. This difference is intriguing and likely points to molecular differences within the CRC cell lines themselves. For example, HT-29 cells express very little endogenous IMP1 (37), so perhaps the signaling paradigm or cellular mediator(s) of IMP1 EV entry are also absent within HT-29 cells. Alternatively, we speculate that reduced levels of m6A methylation may influence whether or not IMP1 enters EVs of specific cell lines as lower levels of m6A could indicate reduced IMP1-mRNA interactions. HT-29 cells express lower levels of m6A methyl transferase METTL3 than SW480 cells (96, 97), suggesting that these cells could have reduced m6A marks. However, Caco2 cells exhibit METTL3 levels similar to those of HT-29 cells (97), suggesting that if m6A marks do influence IMP1 entry in to the EV, this is not the only determinant. If IMP1 is responsible for the transport of key EV cargo in SW480 and Caco2 cell lines, this yet to be defined cargo may be absent from HT-29 cells.

We did observe select IMP1 target mRNAs within EVs isolated from SW480 cells with and without IMP1 expression. *KRAS, MYC, ITGB5,* and *MDRI* were present within the CRC EVs, whereas *PTGS2* was not. This confirms the selectivity with which EV cargo are loaded (15, 82), but also indicates that if IMP1 is involved in carrying these target mRNAs, it is not the only mediator of their EV entry. Other RBPs could also be mediating cargo entry, for example, AGO2 and HuR both enter CRC cell EVs (52, 71) and bind *KRAS* mRNA (33, 98–100), indicating another route for EV *KRAS* loading. Notably, the levels of IMP1 within the SW480 IMP1^{OE} EVs were modest, so differences driven by IMP1 may be difficult to detect in this system. For future studies, a system with more robust IMP1 levels within the EV may more clearly define whether or not IMP1 regulates entry of these or other mRNA cargos.

IMP1 could influence EV cargo beyond mRNA. IMP1 modulates miRNA expression (31, 101, 102) and binds to long noncoding RNAs (103), which could also be transported into EVs (104). It will be important to examine the impacts of IMP1 on all RNA populations when profiling EV cargo in the future.

Our RNA sequencing data indicate that IMP1 expression is associated with increased expression of *MSN* and *SERPINA1*. These proteins have recently been found within EVs isolated from patients with cancer (61, 63). Whether IMP1 directly influences the expression or presence of MSN, SERPINA1, or other protein cargo within EVs is worthy of future investigation.

IMP1 could potentially also play a role in EV tropism. It is reasonable to speculate the EV surface antigen phenotypes may also be affected by IMP1 regulation, which could influence targeting of CRC EVs to specific destinations and/or functions. Proteins present on the EV surface likely govern cell-EV interactions (105, 106). For example, pancreatic cancer EVs with distinct surface integrins seemed to influence organ-specific metastasis to the liver versus the lung (14). IMP1 binds and regulates integrin gene expression, including *ITGB5* (22), therefore it could regulate the expression or presentation of EV-integrins in CRC and direct EV targeting. This could explain why IMP1 expression in primary CRC tumors is associated with nodal metastases (27). The impact of elevated IMP1 levels on CRC EV tropism should be further explored in vivo.

The transfer of functional RBPs via EVs can alter cellular gene expression when the cargo avoids lysosomal degradation (107). Whether IMP1 can be functionally transferred via EVs remains an open question. Future studies should examine if IMP1 is transferred to recipient cells via EVs, if the EV

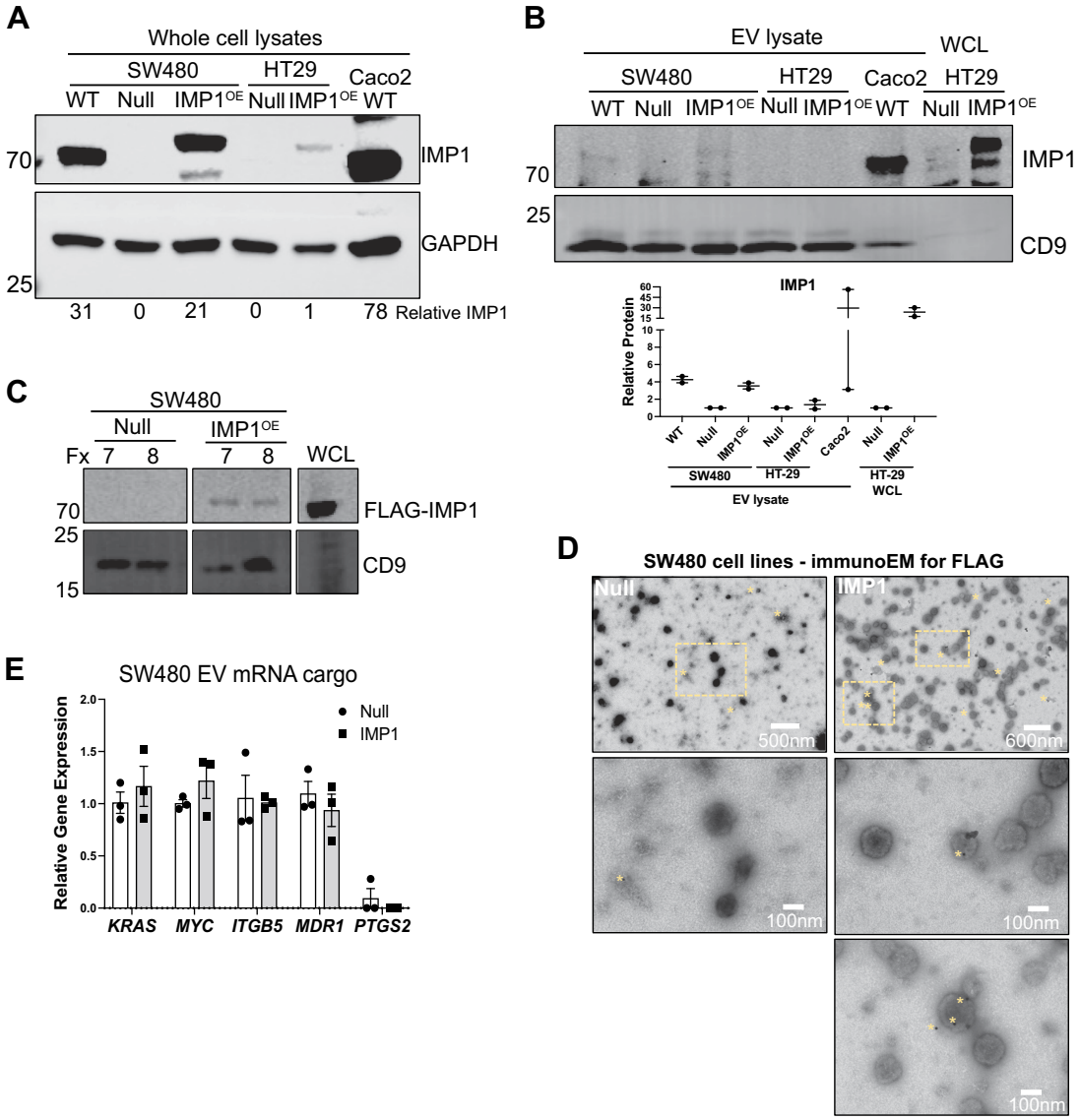

Figure 4. IMP1 enters extracellular vesicles (EV) in select colon cancer cell lines. Western blots using whole cell lysate, 15 μg protein (*A*) or EV lysate (*B*) from SW480 wild-type (WT), IMP1^{Null}, and IMP1^{OE}; HT29 IMP1^{Null} and IMP1^{OE}; and Caco2 cell lines. *A*: relative IMP1 levels were calculated by normalizing IMP1 expression to respective GAPDH levels and then presenting all values as fold-change relative to HT-29 IMP1^{OE}. All densitometry values were calculated using Licor Image Studio Lite v5.2.5. *B*: EVs were isolated from conditioned media by size-exclusion chromatography (SEC). Whole cell lysate (WCL) from HT29 IMP1^{Null} and IMP1^{OE} cell lines are shown as a control. Each lane represents all EVs isolated from conditioned media of four 10-cm dishes for each cell line. Blot is representative of multiple experiments. Dot plot shows IMP1 densitometry values relative to the corresponding null control. Caco2 EV densitometry was normalized to SW480 null EV lysate. Each dot represents a different passage of cells from which EVs were collected. *C*: Western blot for FLAG and CD9 (protein considered to mark EVs) in EVs isolated from SW480 IMP1^{Null} and IMP1^{OE} cell conditioned media. Protein (9 μg) were loaded for all samples. EVs were isolated by SEC, *fractions* (Fx) *7* and *8* are shown. Whole cell lysate (WCL) = HT-29 IMP1^{OE} cells. Data represent a single experiment. *D*: immuno-electron microscopy for FLAG protein in EVs isolated by SEC from SW480 IMP1^{Null} and SW480 IMP1^{OE} cell line conditioned media. Lower magnification images were taken at ×30,000, 500 nm scale bar (null) and ×23,000, 600 nm scale bar IMP1. Boxes indicate zoom images taken at ×98,000 magnification, 100 nm scale bar. *Gold bead. *E*: IMP1 target mRNAs were assessed by qPCR in EVs isolated from SW480 null and IMP1^{OE} cells. EVs isolated by SEC from $n = 3$ independent passages of cells and qPCR reactions run in duplicate for each target and normalized to housekeeping gene *OAZ1* (70). Values are expressed as fold-change relative to null gene expression.

cargo is targeted to the lysosome as previously described for other EVs (108, 109), and if not, how IMP1 delivery alters mRNA stability or expression within the recipient cell.

Interestingly, Ghoshal et al. (24) recently demonstrated that IMP1 expression promotes metastasis in malignant melanoma using differences in EV cargo. Together with our study, this underscores the potential importance of profiling EV cargo secreted from primary tumors with high IMP1 expression. This avenue may lead to early cancer diagnosis and treatment. For example, IMP1's binding to specific target transcripts (*MYC, KRAS*) can be targeted pharmacologically (110, 111).

In summary, we have shown that IMP1 alters the expression of EV pathway related to RNA transcripts, but does not appear to affect EV secretion levels in vitro or in vivo. Instead, its role in CRC EV biology may be related to IMP1

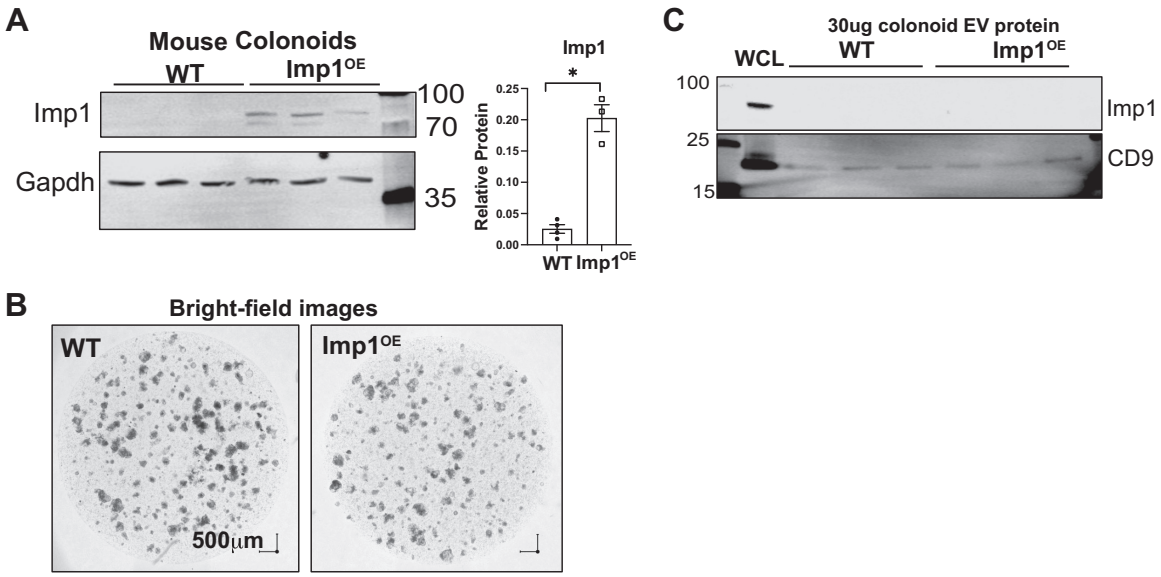

Figure 5. Imp1 does not enter extracellular vesicles isolated from colonoids. Imp1 protein expression was validated by Western blot (*A*) in colonoids derived from wild-type (WT) and Imp1-overexpressing (Imp1^{OE}) mouse colon stem cells, imaged at ×4 (*B*). *C*: conditioned Intesticult media containing particles secreted by colonoids was collected after 48 and 72 h. Extracellular vesicles (EVs) were isolated from conditioned media using size-exclusion chromatography (SEC) and concentrated using Amicon-0.5 concentration column (MWCO 100,000 kDa). The presence of Imp1 and tetraspanin CD9 were examined by Western blot. Whole cell lysate (WCL) controls were SW480 IMP1^{OE} cells. Western blot shows n = 3 colonoid lines.

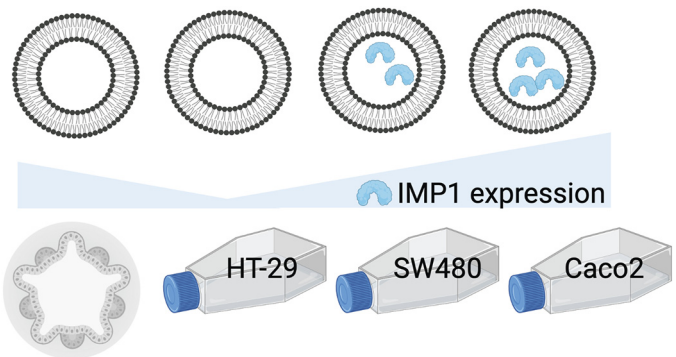

Figure 6. IMP1 enters extracellular vesicles (EVs) secreted from colorectal cancer (CRC) cell lines. IMP1 selectively enters EVs secreted from CRC at relative levels based on cell line IMP1 expression. Imp1 does not enter EVs secreted from nontransformed murine colonoids, despite high Imp1 expression.

incorporation into EVs impacting transcript cargo. Whether these changes are involved in CRC EV targeting or their impact on targeted cells remains to be determined.

SUPPLEMENTAL DATA

Supplemental Figs. S1–S5 and Tables S1–S3: https://doi.org/10.6084/m9.figshare.c.5983702.v1.

ACKNOWLEDGMENTS

We thank Dr. Anil K. Rustgi for generous support and mentorship. We thank Dr. Wei Guo for generous support, helpful discussion, and use of lab space and reagents. We thank members of the Rustgi and Nakagawa labs, Drs. Melissa Wong, and Jonathan Brody for helpful discussions. We thank Dr. Biao Zuo from the Electron Microscopy Resource Lab at the University of Pennsylvania for assistance with TEM staining and imaging. Electron microscopy on SW480 cell EVs and immmunoEM was performed at the Multiscale Microscopy Core (MMC) with the technical assistance of Erin Stempinski and Steven Adamou. The MMC is a member of the OHSU University Shared Resource Cores. Figure diagrams were created with BioRender.com.

GRANTS

Financial support was provided by American Gastroenterological Association Research Scholar Award (to S.F.A.), National Institutes of Health (NIH) NIH F32DK107052 (to S.F.A.), R01 DK056645 (supported S.F.A., K.E.H., and P.S.), R01 DK124369 (to K.E.H.), R35 GM124976 (to P.S.), R01 DK109714 (subcontract to P.S.), R01 DK124369 (subcontract to P.S.), NSF DBI 1936046 (to P.S.), the American Cancer Society (to AK Rustgi supported S.F.A., K.N.W., and K.E.H.), the Lustgarten Family Colon Cancer Fund (to AK Rustgi supported S.F.A., K.N.W., and K.E.H.), Prevent Cancer Foundation Fellowship Award (to R.P.), P30CA13696 (to D.A.D.), R01 CA243445 (to D.A.D), the Knight Cancer Institute (T.K.M.), and startup funds from Oregon Health and Science University (to S.F.A.).

DISCLOSURES

G. Mills is a SAB/Consultant for Amphista, Astex, AstraZeneca, BlueDot, Chrysallis Biotechnology, Ellipses Pharma, GSK, ImmunoMET, Infinity, Ionis, Leapfrog Bio, Lilly, Medacorp, Nanostring, Nuvectis, PDX Pharmaceuticals, Qureator, Roche, Signalchem Lifesciences, Tarveda, Turbine, and Zentalis Pharmaceuticals; Stock/Options/Financial for Bluedot, Catena Pharmaceuticals, ImmunoMet, Nuvectis, SignalChem, Tarveda, Turbine Licensed Technology HRD assay to Myriad Genetics, DSP patents with Nanostring Sponsored research AstraZeneca.

AUTHOR CONTRIBUTIONS

M.M., T.K.M., P.S., and S.F.A. conceived and designed research; M.K., Y.Z., M.M., S.D., S.L., R.P., L.R.P., K.N.W., S.M., R.J.A., W.Z.,

J.Y., T.K.M., and S.F.A. performed experiments; M.K., Y.Z., J.F., M.M., A.B., K.E.H., T.K.M., P.S., and S.F.A., analyzed data; M.K., Y.Z., J.F., M.M., A.B., R.J.A., T.K.M., P.S., and S.F.A. interpreted results of experiments; Y.Z., J.F., M.M., A.B., T.K.M., and S.F.A. prepared figures; M.K., Y.Z., J.F., M.M., A.B., T.K.M., and S.F.A. drafted manuscript; M.K., Y.Z., J.F., M.M., R.P., D.A.D., G.M., T.K.M., P.S., and S.F.A. edited and revised manuscript; M.K., Y.Z., J.F., M.M., A.B., S.D., S.L., R.P., L.R.P., K.N.W., S.M., R.J.A., W.Z., J.Y., K.E.H., D.A.D., G.M., T.K.M., P.S., and S.F.A., approved final version of manuscript.

ENDNOTE

At the request of the authors, readers are herein alerted to the fact that additional materials related to this manuscript may be found at GEO: GSE198804, These materials are not a part of this manuscript and have not undergone peer review by the American Physiological Society (APS). APS and the journal editors take no responsibility for these materials, for the website address, or for any links to or from it.

REFERENCES

1. **Sung H**, **Ferlay J**, **Siegel RL**, **Laversanne M**, **Soerjomataram I**, **Jemal A**, **Bray F.** Global Cancer Statistics 2020: GLOBOCAN estimates of incidence and mortality worldwide for 36 cancers in 185 countries. *CA Cancer J Clin* 71: 209–249, 2021. doi:10.3322/caac.21660.
2. **American Cancer Society.** *Cancer Facts and Figures 2022*. https://www.cancer.org/ [Accessed 2 February 2022].
3. **Loomans-Kropp HA**, **Umar A.** Increasing incidence of colorectal cancer in young adults. *J Cancer Epidemiol* 2019: 9841295, 2019. doi:10.1155/2019/9841295.
4. **Sharpless NE.** COVID-19 and cancer. *Science* 368: 1290, 2020. doi:10.1126/science.abd3377.
5. **Meyerhardt JA**, **Mangu PB**, **Flynn PJ**, **Korde L**, **Loprinzi CL**, **Minsky BD**, **Petrelli NJ**, **Ryan K**, **Schrag DH**, **Wong SL**, **Benson AB 3rd**; **American Society of Clinical Oncology**. Follow-up care, surveillance protocol, and secondary prevention measures for survivors of colorectal cancer: American Society of Clinical Oncology clinical practice guideline endorsement. *J Clin Oncol* 31: 4465–4470, 2013. doi:10.1200/JCO.2013.50.7442.
6. **Siravegna G**, **Marsoni S**, **Siena S**, **Bardelli A.** Integrating liquid biopsies into the management of cancer. *Nat Rev Clin Oncol* 14: 531–548, 2017. doi:10.1038/nrclinonc.2017.14.
7. **Bretthauer M**, **Kaminski MF**, **Loberg M**, **Zauber AG**, **Regula J**, **Kuipers EJ**, **Hernan MA**, **McFadden E**, **Sunde A**, **Kalager M**, **Dekker E**, **Lansdorp-Vogelaar I**, **Garborg K**, **Rupinski M**, **Spaander MC**, **Bugajski M**, **Hoie O**, **Stefansson T**, **Hoff G**, **Adami HO**, **Nordic-European Initiative on Colorectal Cancer (NordICC) Study Group.** Population-based colonoscopy screening for colorectal cancer: a randomized clinical trial. *JAMA Intern Med* 176: 894–902, 2016. doi:10.1001/jamainternmed.2016.0960.
8. **Marcuello M**, **Vymetalkova V**, **Neves RPL**, **Duran-Sanchon S**, **Vedeld HM**, **Tham E**, **van Dalum G**, **Flügen G**, **Garcia-Barberan V**, **Fijneman RJ**, **Castells A**, **Vodicka P**, **Lind GE**, **Stoecklein NH**, **Heitzer E**, **Gironella M.** Circulating biomarkers for early detection and clinical management of colorectal cancer. *Mol Aspects Med* 69: 107–122, 2019. doi:10.1016/j.mam.2019.06.002.
9. **Khan KH**, **Cunningham D**, **Werner B**, **Vlachogiannis G**, **Spiteri I**, **Heide T et al**. Longitudinal liquid biopsy and mathematical modeling of clonal evolution forecast time to treatment failure in the PROSPECT-C phase II colorectal cancer clinical trial. *Cancer Discov* 8: 1270–1285, 2018. doi:10.1158/2159-8290.CD-17-0891.
10. **Liebs S**, **Keilholz U**, **Kehler I**, **Schweiger C**, **Haybäck J**, **Nonnenmacher A.** Detection of mutations in circulating cell-free DNA in relation to disease stage in colorectal cancer. *Cancer Med* 8: 3761–3769, 2019. doi:10.1002/cam4.2219.
11. **Jamaly S**, **Ramberg C**, **Olsen R**, **Latysheva N**, **Webster P**, **Sovershaev T**, **Brækkan SK**, **Hansen J-B.** Impact of preanalytical conditions on plasma concentration and size distribution of extracellular vesicles using Nanoparticle Tracking Analysis. *Sci Rep* 8: 17216, 2018. doi:10.1038/s41598-018-35401-8.
12. **Urabe F**, **Kosaka N**, **Ito K**, **Kimura T**, **Egawa S**, **Ochiya T.** Extracellular vesicles as biomarkers and therapeutic targets for cancer. *Am J Physiol Cell Physiol* 318: C29–C39, 2020. doi:10.1152/ajpcell.00280.2019.
13. **Thery C**, **Witwer KW**, **Aikawa E**, **Alcaraz MJ**, **Anderson JD**, **Andriantsitohaina R**, **et al.** Minimal information for studies of extracellular vesicles 2018 (MISEV2018): a position statement of the International Society for Extracellular Vesicles and update of the MISEV2014 guidelines. *J Extracell Vesicles* 7: 1535750, 2018. doi:10.1080/20013078.2018.1535750.
14. **Hoshino A**, **Costa-Silva B**, **Shen TL**, **Rodrigues G**, **Hashimoto A**, **Tesic Mark M**, **et al.** Tumour exosome integrins determine organotropic metastasis. *Nature* 527: 329–335, 2015. doi:10.1038/nature15756.
15. **Teng Y**, **Ren Y**, **Hu X**, **Mu J**, **Samykutty A**, **Zhuang X**, **Deng Z**, **Kumar A**, **Zhang L**, **Merchant ML**, **Yan J**, **Miller DM**, **Zhang HG.** MVP-mediated exosomal sorting of miR-193a promotes colon cancer progression. *Nat Commun* 8: 14448, 2017. doi:10.1038/ncomms14448.
16. **Wang X**, **Ding X**, **Nan L**, **Wang Y**, **Wang J**, **Yan Z**, **Zhang W**, **Sun J**, **Zhu W**, **Ni B**, **Dong S**, **Yu L.** Investigation of the roles of exosomes in colorectal cancer liver metastasis. *Oncol Rep* 33: 2445–2453, 2015. doi:10.3892/or.2015.3843.
17. **Ganig N**, **Baenke F**, **Thepkaysone ML**, **Lin K**, **Rao VS**, **Wong FC**, **Polster H**, **Schneider M**, **Helm D**, **Pecqueux M**, **Seifert AM**, **Seifert L**, **Weitz J**, **Rahbari NN**, **Kahlert C.** Proteomic analyses of fibroblast- and serum-derived exosomes identify QSOX1 as a marker for non-invasive detection of colorectal cancer. *Cancers (Basel)* 13: 1351, 2021. doi:10.3390/cancers13061351.
18. **Lee CH**, **Im EJ**, **Moon PG**, **Baek MC.** Discovery of a diagnostic biomarker for colon cancer through proteomic profiling of small extracellular vesicles. *BMC Cancer* 18: 1058, 2018. doi:10.1186/s12885-018-4952-y.
19. **Paul D**, **Roy A**, **Nandy A**, **Datta B**, **Borar P**, **Pal SK**, **Senapati D**, **Rakshit T.** Identification of biomarker hyaluronan on colon cancer extracellular vesicles using correlative AFM and spectroscopy. *J Phys Chem Lett* 11: 5569–5576, 2020. doi:10.1021/acs.jpclett.0c01018.
20. **Roman-Canal B**, **Tarragona J**, **Moiola CP**, **Gatius S**, **Bonnin S**, **Ruiz-Miró M**, **Sierra JE**, **Rufas M**, **González E**, **Porcel JM**, **Gil-Moreno A**, **Falcón-Pérez JM**, **Ponomarenko J**, **Matias-Guiu X**, **Colas E.** EV-associated miRNAs from peritoneal lavage as potential diagnostic biomarkers in colorectal cancer. *J Transl Med* 17: 208, 2019. doi:10.1186/s12967-019-1954-8.
21. **Zheng X**, **Xu K**, **Zhou B**, **Chen T**, **Huang Y**, **Li Q**, **Wen F**, **Ge W**, **Wang J**, **Yu S**, **Sun L**, **Zhu L**, **Liu W**, **Gao H**, **Yue L**, **Cai X**, **Zhang Q**, **Ruan G**, **Zhu T**, **Wu Z**, **Zhu Y**, **Shao Y**, **Guo T**, **Zheng S.** A circulating extracellular vesicles-based novel screening tool for colorectal cancer revealed by shotgun and data-independent acquisition mass spectrometry. *J Extracell Vesicles* 9: 1750202, 2020. doi:10.1080/20013078.2020.1750202.
22. **Conway AE**, **Van Nostrand EL**, **Pratt GA**, **Aigner S**, **Wilbert ML**, **Sundararaman B**, **Freese P**, **Lambert NJ**, **Sathe S**, **Liang TY**, **Essex A**, **Landais S**, **Burge CB**, **Jones DL**, **Yeo GW.** Enhanced CLIP uncovers IMP protein-RNA targets in human pluripotent stem cells important for cell adhesion and survival. *Cell Rep* 15: 666–679, 2016. doi:10.1016/j.celrep.2016.03.052.
23. **Fabbiano F**, **Corsi J**, **Gurrieri E**, **Trevisan C**, **Notarangelo M**, **D'Agostino VG.** RNA packaging into extracellular vesicles: an orchestra of RNA-binding proteins? *J Extracell Vesicles* 10: e12043, 2020. doi:10.1002/jev2.12043.
24. **Ghoshal A**, **Rodrigues LC**, **Gowda CP**, **Elcheva IA**, **Liu Z**, **Abraham T**, **Spiegelman VS.** Extracellular vesicle-dependent effect of RNA-binding protein IGF2BP1 on melanoma metastasis. *Oncogene* 38: 4182–4196, 2019. doi:10.1038/s41388-019-0797-3.
25. **Ross J**, **Lemm I**, **Berberet B.** Overexpression of an mRNA-binding protein in human colorectal cancer. *Oncogene* 20: 6544–6550, 2001. doi:10.1038/sj.onc.1204838.
26. **Dimitriadis E**, **Trangas T**, **Milatos S**, **Foukas PG**, **Gioulbasanis I**, **Courtis N**, **Nielsen FC**, **Pandis N**, **Dafni U**, **Bardi G**, **Ioannidis P.** Expression of oncofetal RNA-binding protein CRD-BP/IMP1 predicts clinical outcome in colon cancer. *Int J Cancer* 121: 486–494, 2007. doi:10.1002/ijc.22716.
27. **Madison BB**, **Jeganathan AN**, **Mizuno R**, **Winslow MM**, **Castells A**, **Cuatrecasas M**, **Rustgi AK.** Let-7 represses carcinogenesis and a stem cell phenotype in the intestine via regulation of Hmga2. *PLoS Genet* 11: e1005408, 2015. doi:10.1371/journal.pgen.1005408.

28. **Bell JL**, **Wächter K**, **Muhleck B**, **Pazaitis N**, **Köhn M**, **Lederer M**, **Hüttelmaier S.** Insulin-like growth factor 2 mRNA-binding proteins (IGF2BPs): post-transcriptional drivers of cancer progression? *Cell Mol Life Sci* 70: 2657–2675, 2013. doi:10.1007/s00018-012-1186-z.
29. **Huang H**, **Weng H**, **Sun W**, **Qin X**, **Shi H**, **Wu H**, **Zhao BS**, **Mesquita A**, **Liu C**, **Yuan CL**, **Hu Y-C**, **Hüttelmaier S**, **Skibbe JR**, **Su R**, **Deng X**, **Dong L**, **Sun M**, **Li C**, **Nachtergaele S**, **Wang Y**, **Hu C**, **Ferchen K**, **Greis KD**, **Jiang X**, **Wei M**, **Qu L**, **Guan J-L**, **He C**, **Yang J**, **Chen J.** Recognition of RNA N(6)-methyladenosine by IGF2BP proteins enhances mRNA stability and translation. *Nat Cell Biol* 20: 285–295, 2018. doi:10.1038/s41556-018-0045-z.
30. **Hubstenberger A**, **Courel M**, **Bénard M**, **Souquere S**, **Ernoult-Lange M**, **Chouaib R**, **Yi Z**, **Morlot JB**, **Munier A**, **Fradet M**, **Daunesse M**, **Bertrand E**, **Pierron G**, **Mozziconacci J**, **Kress M**, **Weil D.** P-body purification reveals the condensation of repressed mRNA regulons. *Mol Cell* 68: 144–157.e5, 2017. doi:10.1016/j.molcel.2017.09.003.
31. **Müller S**, **Bley N**, **Glaß M**, **Busch B**, **Rousseau V**, **Misiak D**, **Fuchs T**, **Lederer M**, **Hüttelmaier S.** IGF2BP1 enhances an aggressive tumor cell phenotype by impairing miRNA-directed downregulation of oncogenic factors. *Nucleic Acids Res* 46: 6285–6303, 2018. doi:10.1093/nar/gky229.
32. **Stöhr N**, **Lederer M**, **Reinke C**, **Meyer S**, **Hatzfeld M**, **Singer RH**, **Hüttelmaier S.** ZBP1 regulates mRNA stability during cellular stress. *J Cell Biol* 175: 527–534, 2006. doi:10.1083/jcb.200608071.
33. **Hafner M**, **Landthaler M**, **Burger L**, **Khorshid M**, **Hausser J**, **Berninger P**, **Rothballer A**, **Ascano M Jr**, **Jungkamp AC**, **Munschauer M**, **Ulrich A**, **Wardle GS**, **Dewell S**, **Zavolan M**, **Tuschl T.** Transcriptome-wide identification of RNA-binding protein and microRNA target sites by PAR-CLIP. *Cell* 141: 129–141, 2010. doi:10.1016/j.cell.2010.03.009.
34. **Meyer KD**, **Saletore Y**, **Zumbo P**, **Elemento O**, **Mason CE**, **Jaffrey SR.** Comprehensive analysis of mRNA methylation reveals enrichment in 3' UTRs and near stop codons. *Cell* 149: 1635–1646, 2012. doi:10.1016/j.cell.2012.05.003.
35. **Dominissini D**, **Moshitch-Moshkovitz S**, **Schwartz S**, **Salmon-Divon M**, **Ungar L**, **Osenberg S**, **Cesarkas K**, **Jacob-Hirsch J**, **Amariglio N**, **Kupiec M**, **Sorek R**, **Rechavi G.** Topology of the human and mouse m6A RNA methylomes revealed by m6A-seq. *Nature* 485: 201–206, 2012. doi:10.1038/nature11112.
36. **Liu N**, **Dai Q**, **Zheng G**, **He C**, **Parisien M**, **Pan T.** N(6)-methyladenosine-dependent RNA structural switches regulate RNA-protein interactions. *Nature* 518: 560–564, 2015. doi:10.1038/nature14234.
37. **Mongroo PS**, **Noubissi FK**, **Cuatrecasas M**, **Kalabis J**, **King CE**, **Johnstone CN**, **Bowser MJ**, **Castells A**, **Spiegelman VS**, **Rustgi AK.** IMP-1 displays cross-talk with K-Ras and modulates colon cancer cell survival through the novel proapoptotic protein CYFIP2. *Cancer Res* 71: 2172–2182, 2011. doi:10.1158/0008-5472.CAN-10-3295.
38. **Lemm I**, **Ross J.** Regulation of c-myc mRNA decay by translational pausing in a coding region instability determinant. *Mol Cell Biol* 22: 3959–3969, 2002. doi:10.1128/MCB.22.12.3959-3969.2002.
39. **Noubissi FK**, **Elcheva I**, **Bhatia N**, **Shakoori A**, **Ougolkov A**, **Liu J**, **Minamoto T**, **Ross J**, **Fuchs SY**, **Spiegelman VS.** CRD-BP mediates stabilization of βTrCP1 and c-myc mRNA in response to beta-catenin signalling. *Nature* 441: 898–901, 2006. doi:10.1038/nature04839.
40. **Vikesaa J**, **Hansen TV**, **Jønson L**, **Borup R**, **Wewer UM**, **Christiansen J**, **Nielsen FC.** RNA-binding IMPs promote cell adhesion and invadopodia formation. *EMBO J* 25: 1456–1468, 2006. doi:10.1038/sj.emboj.7601039.
41. **Manieri NA**, **Drylewicz MR**, **Miyoshi H**, **Stappenbeck TS.** Igf2bp1 is required for full induction of Ptgs2 mRNA in colonic mesenchymal stem cells in mice. *Gastroenterology* 143: 110–121.e10, 2012. doi:10.1053/j.gastro.2012.03.037.
42. **Sparanese D**, **Lee CH.** CRD-BP shields c-myc and MDR-1 RNA from endonucleolytic attack by a mammalian endoribonuclease. *Nucleic Acids Res* 35: 1209–1221, 2007. doi:10.1093/nar/gkl1148.
43. **Andres SF**, **Williams KN**, **Plesset JB**, **Headd JJ**, **Mizuno R**, **Chatterji P**, **Lento AA**, **Klein-Szanto AJ**, **Mick R**, **Hamilton KE**, **Rustgi AK.** IMP1 3'UTR shortening enhances metastatic burden in colorectal cancer. *Carcinogenesis* 40: 569–579, 2019. doi:10.1093/carcin/bgy153.
44. **Chatterji P**, **Hamilton KE**, **Liang S**, **Andres SF**, **Wijeratne HRS**, **Mizuno R**, **Simon LA**, **Hicks PD**, **Foley SW**, **Pitarresi JR**, **Klein-Szanto AJ**, **Mah AT**, **Van Landeghem L**, **Gregory BD**, **Lengner CJ**, **Madison BB**, **Shah P**, **Rustgi AK.** The LIN28B-IMP1 post-transcriptional regulon has opposing effects on oncogenic signaling in the intestine. *Genes Dev* 32: 1020–1034, 2018. doi:10.1101/gad.314369.118.
45. **Mizutani T**, **Clevers H.** Primary intestinal epithelial organoid culture. *Methods Mol Biol* 2171: 185–200, 2020. doi:10.1007/978-1-0716-0747-3_11.
46. **Martin M.** Cutadapt removes adapter sequences from high-throughput sequencing reads. *EMBnet j* 17: 10–12, 2011. doi:10.14806/ej.17.1.200.
47. **Bray NL**, **Pimentel H**, **Melsted P**, **Pachter L.** Near-optimal probabilistic RNA-seq quantification. *Nat Biotechnol* 34: 525–527, 2016. doi:10.1038/nbt.3519.
48. **Rodriguez JM**, **Rodriguez-Rivas J**, **Di Domenico T**, **Vázquez J**, **Valencia A**, **Tress ML.** APPRIS 2017: principal isoforms for multiple gene sets. *Nucleic Acids Res* 46: D213–D217, 2018. doi:10.1093/nar/gkx997.
49. **Love MI**, **Huber W**, **Anders S.** Moderated estimation of fold change and dispersion for RNA-seq data with DESeq2. *Genome Biol* 15: 550, 2014. doi:10.1186/s13059-014-0550-8.
50. **Ashburner M**, **Ball CA**, **Blake JA**, **Botstein D**, **Butler H**, **Cherry JM**, **Davis AP**, **Dolinski K**, **Dwight SS**, **Eppig JT**, **Harris MA**, **Hill DP**, **Issel-Tarver L**, **Kasarskis A**, **Lewis S**, **Matese JC**, **Richardson JE**, **Ringwald M**, **Rubin GM**, **Sherlock G.** Gene ontology: tool for the unification of biology. The Gene Ontology Consortium. *Nat Genet* 25: 25–29, 2000. doi:10.1038/75556.
51. **The Gene Ontology Consortium.** The Gene Ontology Resource: 20 years and still GOing strong. *Nucleic Acids Res* 47: D330–D338, 2019. doi:10.1093/nar/gky1055.
52. **Xiao H**, **Ye X**, **Vishwakarma V**, **Preet R**, **Dixon DA.** CRC-derived exosomes containing the RNA binding protein HuR promote lung cell proliferation by stabilizing c-Myc mRNA. *Cancer Biol Ther* 23: 139–149, 2022. doi:10.1080/15384047.2022.2034455.
53. R Core **Team.** R: A Language and Environment for Statistical Computing. Vienna, Austria: R Foundation for Statistical Computing, 2022. https://www.r-project.org
54. **Clemente L**, **Boeldt DS**, **Grummer MA**, **Morita M**, **Morgan TK**, **Wiepz GJ**, **Bertics PJ**, **Bird IM.** Adenoviral transduction of EGFR into pregnancy-adapted uterine artery endothelial cells remaps growth factor induction of endothelial dysfunction. *Mol Cell Endocrinol* 499: 110590, 2020. doi:10.1016/j.mce.2019.110590.
55. **Mitrugno A**, **Tassi Yunga S**, **Sylman JL**, **Zilberman-Rudenko J**, **Shirai T**, **Hebert JF**, **Kayton R**, **Zhang Y**, **Nan X**, **Shatzel JJ**, **Esener S**, **Duvernay MT**, **Hamm HE**, **Gruber A**, **Williams CD**, **Takata Y**, **Armstrong R**, **Morgan TK**, **McCarty OJT.** The role of coagulation and platelets in colon cancer-associated thrombosis. *Am J Physiol Cell Physiol* 316: C264–C273, 2019. doi:10.1152/ajpcell.00367.2018.
56. **Morgan TK.** Cell- and size-specific analysis of placental extracellular vesicles in maternal plasma and pre-eclampsia. *Transl Res* 201: 40–48, 2018. doi:10.1016/j.trsl.2018.08.004.
57. **Trainer DL**, **Kline T**, **McCabe FL**, **Faucette LF**, **Feild J**, **Chaikin M**, **Anzano M**, **Rieman D**, **Hoffstein S**, **Li DJ.** Biological characterization and oncogene expression in human colorectal carcinoma cell lines. *Int J Cancer* 41: 287–296, 1988. doi:10.1002/ijc.2910410221.
58. **Nielsen J**, **Christiansen J**, **Lykke-Andersen J**, **Johnsen AH**, **Wewer UM**, **Nielsen FC.** A family of insulin-like growth factor II mRNA-binding proteins represses translation in late development. *Mol Cell Biol* 19: 1262–1270, 1999. doi:10.1128/MCB.19.2.1262.
59. **Wang G**, **Huang Z**, **Liu X**, **Huang W**, **Chen S**, **Zhou Y**, **Li D**, **Singer RH**, **Gu W.** IMP1 suppresses breast tumor growth and metastasis through the regulation of its target mRNAs. *Oncotarget* 7: 15690–15702, 2016. doi:10.18632/oncotarget.7464.
60. **Kowal J**, **Arras G**, **Colombo M**, **Jouve M**, **Morath JP**, **Primdal-Bengtson B**, **Dingli F**, **Loew D**, **Tkach M**, **Théry C.** Proteomic comparison defines novel markers to characterize heterogeneous populations of extracellular vesicle subtypes. *Proc Natl Acad Sci USA* 113: E968–E977, 2016. doi:10.1073/pnas.1521230113.
61. **Hoshino A**, **Kim HS**, **Bojmar L**, **Gyan KE**, **Cioffi M**, **Hernandez J et al.** Extracellular vesicle and particle biomarkers define multiple human cancers. *Cell* 182: 1044–1061.e18, 2020. doi:10.1016/j.cell.2020.07.009.
62. **Choi DS**, **Choi DY**, **Hong BS**, **Jang SC**, **Kim DK**, **Lee J**, **Kim YK**, **Kim KP**, **Gho YS.** Quantitative proteomics of extracellular vesicles derived from human primary and metastatic colorectal cancer cells. *J Extracell Vesicles* 1: 1, 2012. doi:10.3402/jev.v1i0.18704.
63. **Chen Y**, **Xie Y**, **Xu L**, **Zhan S**, **Xiao Y**, **Gao Y**, **Wu B**, **Ge W.** Protein content and functional characteristics of serum-purified exosomes

from patients with colorectal cancer revealed by quantitative proteomics. *Int J Cancer* 140: 900–913, 2017. doi:10.1002/ijc.30496.
64. **Clarke-Bland CE**, **Bill RM**, **Devitt A.** Emerging roles for AQP in mammalian extracellular vesicles. *Biochim Biophys Acta Biomembr* 1864: 183826, 2022. doi:10.1016/j.bbamem.2021.183826.
65. **Muriel O**, **Tomas A**, **Scott CC**, **Gruenberg J.** Moesin and cortactin control actin-dependent multivesicular endosome biogenesis. *Mol Biol Cell* 27: 3305–3316, 2016. doi:10.1091/mbc.E15-12-0853.
66. **Uytterhoeven V**, **Lauwers E**, **Maes I**, **Miskiewicz K**, **Melo MN**, **Swerts J**, **Kuenen S**, **Wittocx R**, **Corthout N**, **Marrink SJ**, **Munck S**, **Verstreken P.** Hsc70-4 deforms membranes to promote synaptic protein turnover by endosomal microautophagy. *Neuron* 88: 735–748, 2015. doi:10.1016/j.neuron.2015.10.012.
67. **Colombo M**, **Raposo G**, **Théry C.** Biogenesis, secretion, and intercellular interactions of exosomes and other extracellular vesicles. *Annu Rev Cell Dev Biol* 30: 255–289, 2014. doi:10.1146/annurev-cellbio-101512-122326.
68. **Ostrowski M**, **Carmo NB**, **Krumeich S**, **Fanget I**, **Raposo G**, **Savina A**, **Moita CF**, **Schauer K**, **Hume AN**, **Freitas RP**, **Goud B**, **Benaroch P**, **Hacohen N**, **Fukuda M**, **Desnos C**, **Seabra MC**, **Darchen F**, **Amigorena S**, **Moita LF**, **Thery C.** Rab27a and Rab27b control different steps of the exosome secretion pathway. *Nat Cell Biol* 12: 19–30, 2010. doi:10.1038/ncb2000.
69. **Sullivan R**, **Maresh G**, **Zhang X**, **Salomon C**, **Hooper J**, **Margolin D**, **Li L.** The emerging roles of extracellular vesicles as communication vehicles within the tumor microenvironment and beyond. *Front Endocrinol (Lausanne)* 8: 194, 2017. doi:10.3389/fendo.2017.00194.
70. **Dai Y**, **Cao Y**, **Köhler J**, **Lu A**, **Xu S**, **Wang H.** Unbiased RNA-Seq-driven identification and validation of reference genes for quantitative RT-PCR analyses of pooled cancer exosomes. *BMC Genomics* 22: 27, 2021. doi:10.1186/s12864-020-07318-y.
71. **McKenzie AJ**, **Hoshino D**, **Hong NH**, **Cha DJ**, **Franklin JL**, **Coffey RJ**, **Patton JG**, **Weaver AM.** KRAS-MEK signaling controls Ago2 sorting into exosomes. *Cell Rep* 15: 978–987, 2016. doi:10.1016/j.celrep.2016.03.085.
72. **Hansen TV**, **Hammer NA**, **Nielsen J**, **Madsen M**, **Dalbaeck C**, **Wewer UM**, **Christiansen J**, **Nielsen FC.** Dwarfism and impaired gut development in insulin-like growth factor II mRNA-binding protein 1-deficient mice. *Mol Cell Biol* 24: 4448–4464, 2004. doi:10.1128/MCB.24.10.4448-4464.2004.
73. **Rosenfeld YB**, **Krumbein M**, **Yeffet A**, **Schiffmann N**, **Mishalian I**, **Pikarsky E**, **Oberman F**, **Fridlender Z**, **Yisraeli JK.** VICKZ1 enhances tumor progression and metastasis in lung adenocarcinomas in mice. *Oncogene* 38: 4169–4181, 2019. doi:10.1038/s41388-019-0715-8.
74. **Bernstein PL**, **Herrick DJ**, **Prokipcak RD**, **Ross J.** Control of c-myc mRNA half-life in vitro by a protein capable of binding to a coding region stability determinant. *Genes Dev* 6: 642–654, 1992. doi:10.1101/gad.6.4.642.
75. **Prokipcak RD**, **Herrick DJ**, **Ross J.** Purification and properties of a protein that binds to the C-terminal coding region of human c-myc mRNA. *J Biol Chem* 269: 9261–9269, 1994. doi:10.1016/S0021-9258(17)37102-8.
76. **Noubissi FK**, **Goswami S**, **Sanek NA**, **Kawakami K**, **Minamoto T**, **Moser A**, **Grinblat Y**, **Spiegelman VS.** Wnt signaling stimulates transcriptional outcome of the Hedgehog pathway by stabilizing GLI1 mRNA. *Cancer Res* 69: 8572–8578, 2009. doi:10.1158/0008-5472.CAN-09-1500.
77. **Lv D**, **Ding S**, **Zhong L**, **Tu J**, **Li H**, **Yao H**, **Zou Y**, **Zeng Z**, **Liao Y**, **Wan X**, **Wen L**, **Xie X.** M6A demethylase FTO-mediated downregulation of DACT1 mRNA stability promotes Wnt signaling to facilitate osteosarcoma progression. *Oncogene* 41: 1727–1741, 2022. doi:10.1038/s41388-022-02214-z.
78. **Szvicsek Z**, **Oszvald Á**, **Szabó L**, **Sándor GO**, **Kelemen A**, **Soós AÁ**, **Pálóczi K**, **Harsányi L**, **Tölgyes T**, **Dede K**, **Bursics A**, **Buzás EI**, **Zeöld A**, **Wiener Z.** Extracellular vesicle release from intestinal organoids is modulated by Apc mutation and other colorectal cancer progression factors. *Cell Mol Life Sci* 76: 2463–2476, 2019. doi:10.1007/s00018-019-03052-1.
79. **Sexton RE**, **Mpilla G**, **Kim S**, **Philip PA**, **Azmi AS.** Ras and exosome signaling. *Semin Cancer Biol* 54: 131–137, 2019. doi:10.1016/j.semcancer.2019.02.004.
80. **Lee TH**, **Chennakrishnaiah S**, **Audemard E**, **Montermini L**, **Meehan B**, **Rak J.** Oncogenic ras-driven cancer cell vesiculation leads to emission of double-stranded DNA capable of interacting with target cells. *Biochem Biophys Res Commun* 451: 295–301, 2014. doi:10.1016/j.bbrc.2014.07.109.
81. **Demory Beckler M**, **Higginbotham JN**, **Franklin JL**, **Ham AJ**, **Halvey PJ**, **Imasuen IE**, **Whitwell C**, **Li M**, **Liebler DC**, **Coffey RJ.** Proteomic analysis of exosomes from mutant KRAS colon cancer cells identifies intercellular transfer of mutant KRAS. *Mol Cell Proteomics* 12: 343–355, 2013. doi:10.1074/mcp.M112.022806.
82. **Cha DJ**, **Franklin JL**, **Dou Y**, **Liu Q**, **Higginbotham JN**, **Demory Beckler M**, **Weaver AM**, **Vickers K**, **Prasad N**, **Levy S**, **Zhang B**, **Coffey RJ**, **Patton JG.** KRAS-dependent sorting of miRNA to exosomes. *eLife* 4: e07197, 2015. doi:10.7554/eLife.07197.
83. **Hinger SA**, **Abner JJ**, **Franklin JL**, **Jeppesen DK**, **Coffey RJ**, **Patton JG.** Rab13 regulates sEV secretion in mutant KRAS colorectal cancer cells. *Sci Rep* 10: 15804, 2020. doi:10.1038/s41598-020-72503-8.
84. **Pyzer AR**, **Stroopinsky D**, **Rajabi H**, **Washington A**, **Tagde A**, **Coll M**, **Fung J**, **Bryant MP**, **Cole L**, **Palmer K**, **Somaiya P**, **Karp Leaf R**, **Nahas M**, **Apel A**, **Jain S**, **McMasters M**, **Mendez L**, **Levine J**, **Joyce R**, **Arnason J**, **Pandolfi PP**, **Kufe D**, **Rosenblatt J**, **Avigan D.** MUC1-mediated induction of myeloid-derived suppressor cells in patients with acute myeloid leukemia. *Blood* 129: 1791–1801, 2017. doi:10.1182/blood-2016-07-730614.
85. **Chatterji P**, **Williams PA**, **Whelan KA**, **Samper FC**, **Andres SF**, **Simon LA**, **Parham LR**, **Mizuno R**, **Lundsmith ET**, **Lee DS**, **Liang S**, **Wijeratne HS**, **Marti S**, **Chau L**, **Giroux V**, **Wilkins BJ**, **Wu GD**, **Shah P**, **Tartaglia GG**, **Hamilton KE.** Posttranscriptional regulation of colonic epithelial repair by RNA binding protein IMP1/IGF2BP1. *EMBO Rep* 20, 2019. doi:10.15252/embr.201847074.
86. **Bhattacharya S**, **Pal K**, **Sharma AK**, **Dutta SK**, **Lau JS**, **Yan IK**, **Wang E**, **Elkhanany A**, **Alkharfy KM**, **Sanyal A**, **Patel TC**, **Chari ST**, **Spaller MR**, **Mukhopadhyay D.** GAIP interacting protein C-terminus regulates autophagy and exosome biogenesis of pancreatic cancer through metabolic pathways. *PLoS One* 9: e114409, 2014. doi:10.1371/journal.pone.0114409.
87. **Kanemoto S**, **Nitani R**, **Murakami T**, **Kaneko M**, **Asada R**, **Matsuhisa K**, **Saito A**, **Imaizumi K.** Multivesicular body formation enhancement and exosome release during endoplasmic reticulum stress. *Biochem Biophys Res Commun* 480: 166–172, 2016. doi:10.1016/j.bbrc.2016.10.019.
88. **Kumar D**, **Gupta D**, **Shankar S**, **Srivastava RK.** Biomolecular characterization of exosomes released from cancer stem cells: possible implications for biomarker and treatment of cancer. *Oncotarget* 6: 3280–3291, 2015. doi:10.18632/oncotarget.2462.
89. **Murrow L**, **Malhotra R**, **Debnath J.** ATG12-ATG3 interacts with Alix to promote basal autophagic flux and late endosome function. *Nat Cell Biol* 17: 300–310, 2015. doi:10.1038/ncb3112.
90. **Fader CM**, **Sánchez D**, **Furlán M**, **Colombo MI.** Induction of autophagy promotes fusion of multivesicular bodies with autophagic vacuoles in k562 cells. *Traffic* 9: 230–250, 2008. doi:10.1111/j.1600-0854.2007.00677.x.
91. **Hurwitz SN**, **Cheerathodi MR**, **Nkosi D**, **York SB**, **Meckes DG Jr.** Tetraspanin CD63 bridges autophagic and endosomal processes to regulate exosomal secretion and intracellular signaling of Epstein–Barr virus LMP1. *J Virol* 92: e01969-17, 2018. doi:10.1128/JVI.01969-17.
92. **Takahashi A**, **Okada R**, **Nagao K**, **Kawamata Y**, **Hanyu A**, **Yoshimoto S**, **Takasugi M**, **Watanabe S**, **Kanemaki MT**, **Obuse C**, **Hara E.** Exosomes maintain cellular homeostasis by excreting harmful DNA from cells. *Nat Commun* 8: 15287, 2017 [Erratum in *Nat Commun* 9: 4109, 2018]. doi:10.1038/ncomms15287.
93. **Villarroya-Beltri C**, **Baixauli F**, **Mittelbrunn M**, **Fernández-Delgado I**, **Torralba D**, **Moreno-Gonzalo O**, **Baldanta S**, **Enrich C**, **Guerra S**, **Sánchez-Madrid F.** ISGylation controls exosome secretion by promoting lysosomal degradation of MVB proteins. *Nat Commun* 7: 13588, 2016. doi:10.1038/ncomms13588.
94. **Guo H**, **Chitiprolu M**, **Roncevic L**, **Javalet C**, **Hemming FJ**, **Trung MT**, **Meng L**, **Latreille E**, **Tanese de Souza C**, **McCulloch D**, **Baldwin RM**, **Auer R**, **Côté J**, **Russell RC**, **Sadoul R**, **Gibbings D.** Atg5 disassociates the V1V0-ATPase to promote exosome production and tumor metastasis independent of canonical macroautophagy. *Dev Cell* 43: 716–730.e7, 2017. doi:10.1016/j.devcel.2017.11.018.
95. **Gudbergsson JM**, **Johnsen KB.** Exosomes and autophagy: rekindling the vesicular waste hypothesis. *J Cell Commun Signal* 13: 443–450, 2019. doi:10.1007/s12079-019-00524-8.
96. **Wen J**, **Zhang G**, **Meng Y**, **Zhang L**, **Jiang M**, **Yu Z.** RNA m(6)A methyltransferase METTL3 promotes colorectal cancer cell proliferation

and invasion by regulating Snail expression. *Oncol Lett* 22: 711, 2021. doi:10.3892/ol.2021.12972.

97. **Xiang S**, **Liang X**, **Yin S**, **Liu J**, **Xiang Z.** N6-methyladenosine methyltransferase METTL3 promotes colorectal cancer cell proliferation through enhancing MYC expression. *Am J Transl Res* 12: 1789–1806, 2020.
98. **Kishore S**, **Jaskiewicz L**, **Burger L**, **Hausser J**, **Khorshid M**, **Zavolan M.** A quantitative analysis of CLIP methods for identifying binding sites of RNA-binding proteins. *Nat Methods* 8: 559–564, 2011. doi:10.1038/nmeth.1608.
99. **Lebedeva S**, **Jens M**, **Theil K**, **Schwanhäusser B**, **Selbach M**, **Landthaler M**, **Rajewsky N.** Transcriptome-wide analysis of regulatory interactions of the RNA-binding protein HuR. *Mol Cell* 43: 340–352, 2011. doi:10.1016/j.molcel.2011.06.008.
100. **Mukherjee N**, **Corcoran DL**, **Nusbaum JD**, **Reid DW**, **Georgiev S**, **Hafner M**, **Ascano M Jr**, **Tuschl T**, **Ohler U**, **Keene JD.** Integrative regulatory mapping indicates that the RNA-binding protein HuR couples pre-mRNA processing and mRNA stability. *Mol Cell* 43: 327–339, 2011. doi:10.1016/j.molcel.2011.06.007.
101. **Degrauwe N**, **Suvà ML**, **Janiszewska M**, **Riggi N**, **Stamenkovic I.** IMPs: an RNA-binding protein family that provides a link between stem cell maintenance in normal development and cancer. *Genes Dev* 30: 2459–2474, 2016. doi:10.1101/gad.287540.116.
102. **Busch B**, **Bley N**, **Müller S**, **Glaß M**, **Misiak D**, **Lederer M**, **Vetter M**, **Strauß H-G**, **Thomssen C**, **Hüttelmaier S.** The oncogenic triangle of HMGA2, LIN28B and IGF2BP1 antagonizes tumor-suppressive actions of the let-7 family. *Nucleic Acids Res* 44: 3845–3864, 2016. doi:10.1093/nar/gkw099.
103. **Zhu P**, **He F**, **Hou Y**, **Tu G**, **Li Q**, **Jin T**, **Zeng H**, **Qin Y**, **Wan X**, **Qiao Y**, **Qiu Y**, **Teng Y**, **Liu M.** A novel hypoxic long noncoding RNA KB-1980E6.3 maintains breast cancer stem cell stemness via interacting with IGF2BP1 to facilitate c-Myc mRNA stability. *Oncogene* 40: 1609–1627, 2021. doi:10.1038/s41388-020-01638-9.
104. **Valadi H**, **Ekström K**, **Bossios A**, **Sjöstrand M**, **Lee JJ**, **Lötvall JO.** Exosome-mediated transfer of mRNAs and microRNAs is a novel mechanism of genetic exchange between cells. *Nat Cell Biol* 9: 654–659, 2007. doi:10.1038/ncb1596.
105. **Morelli AE**, **Larregina AT**, **Shufesky WJ**, **Sullivan ML**, **Stolz DB**, **Papworth GD**, **Zahorchak AF**, **Logar AJ**, **Wang Z**, **Watkins SC**, **Falo LD Jr**, **Thomson AW.** Endocytosis, intracellular sorting, and processing of exosomes by dendritic cells. *Blood* 104: 3257–3266, 2004. doi:10.1182/blood-2004-03-0824.
106. **Purushothaman A**, **Bandari SK**, **Liu J**, **Mobley JA**, **Brown EE**, **Sanderson RD.** Fibronectin on the surface of myeloma cell-derived exosomes mediates exosome-cell interactions. *J Biol Chem* 291: 1652–1663, 2016. doi:10.1074/jbc.M115.686295.
107. **Pavlyukov MS**, **Yu H**, **Bastola S**, **Minata M**, **Shender VO**, **Lee Y**, **Zhang S**, **Wang J**, **Komarova S**, **Wang J**, **Yamaguchi S**, **Alsheikh HA**, **Shi J**, **Chen D**, **Mohyeldin A**, **Kim SH**, **Shin YJ**, **Anufrieva K**, **Evtushenko EG**, **Antipova NV**, **Arapidi GP**, **Govorun V**, **Pestov NB**, **Shakhparonov MI**, **Lee LJ**, **Nam DH**, **Nakano I.** Apoptotic cell-derived extracellular vesicles promote malignancy of glioblastoma via intercellular transfer of splicing factors. *Cancer Cell* 34: 119–135. e10, 2018. doi:10.1016/j.ccell.2018.05.012.
108. **Choi D**, **Montermini L**, **Meehan B**, **Lazaris A**, **Metrakos P**, **Rak J.** Oncogenic RAS drives the CRAF-dependent extracellular vesicle uptake mechanism coupled with metastasis. *J Extracell Vesicles* 10: e12091, 2021. doi:10.1002/jev2.12091.
109. **Montermini L**, **Meehan B**, **Garnier D**, **Lee WJ**, **Lee TH**, **Guha A**, **Al-Nedawi K**, **Rak J.** Inhibition of oncogenic epidermal growth factor receptor kinase triggers release of exosome-like extracellular vesicles and impacts their phosphoprotein and DNA content. *J Biol Chem* 290: 24534–24546, 2015. doi:10.1074/jbc.M115.679217.
110. **Mahapatra L**, **Andruska N**, **Mao C**, **Le J**, **Shapiro DJ.** A novel IMP1 inhibitor, BTYNB, targets c-Myc and inhibits melanoma and ovarian cancer cell proliferation. *Transl Oncol* 10: 818–827, 2017. doi:10.1016/j.tranon.2017.07.008.
111. **Wallis N**, **Oberman F**, **Shurrush K**, **Germain N**, **Greenwald G**, **Gershon T**, **Pearl T**, **Abis G**, **Singh V**, **Singh A**, **Sharma AK**, **Barr HM**, **Ramos A**, **Spiegelman VS**, **Yisraeli JK.** Small molecule inhibitor of Igf2bp1 represses Kras and a pro-oncogenic phenotype in cancer cells. *RNA Biol* 19: 26–43, 2022. doi:10.1080/15476286.2021.2010983.